Methods for Analysis of Preliminary Spacecraft Designs
AAE450, Spacecraft Design, Purdue University

Written by Steven P. Schneider
Associate Professor
Adapted from Methods Developed by W. Gustafson
Professor Emeritus
School of Aeronautics and Astronautics
Purdue University

August 18, 2003

Contents

1 Introduction

The following is a collection of notes describing the methods used for analysis of preliminary designs, in the senior capstone Spacecraft Design course at Purdue University. These notes were first collected in Fall 1999. They are preliminary, and subject to continual revision. Please inform the author of any errors you may detect.

It is very important to realize that for preliminary design, you just try to get the big picture. The analysis methods used here need only be accurate and reliable enough to give a correct idea

of the general tradeoffs between vehicle size, shape, trajectory, and so on. During the preliminary design, you should accumulate a list of details that need to be verified later. The main effort is to determine the validity of the overall concept, and attempt to be sure that you aren't missing any 'show-stoppers'.

Your vehicle design and the supporting analysis will end up embodied in a computer program. This program will both define your vehicle and serve to implement the analysis of its performance. A number of such programs are available from previous semesters (beginning in Fall 1998) to serve as a basis for your designs (see the public-access course directory). The instructor's sample programs are also available in the subdirectory `/sps_prgm`. See also the AAE450 website (Prof. Schneider's section, possibly still located under the Spacecraft part of the 451 website at `http://roger.ecn.purdue.edu/ aae450s/`).

Should you choose to begin with an existing code, you can take advantage of previous efforts, as one normally does. However, you are then responsible for the accuracy of the codes, so check them carefully for bugs! Since your code is used to demonstrate the performance of your design, any errors in the coded analysis make your performance results dubious at best. Your codes should thus be well documented and well checked. Any past codes that you use should be well understood, and improved. Put your name and the last date of modification at the top of the code. Use generous commenting to describe the variables and the logic. All equations coded in the program should have comments referring to the text, handout, or section of your report in which the equations are written out or described. `FORTRAN` will continue to be used as the main language for this course, allowing continued use of the existing code base and of the instructor's expertise in that language. You may need to refresh your knowledge by picking up a reference book and studying it. **All of your analysis should be traceable back to standard engineering methods, either through references to standard works or detailed presentations of your own.** Don't reinvent the wheel, but do refer equations back to their source, so they can be checked.

Reports from previous semesters are on file in the Design Room in Grissom 100. It may be profitable to consult these when performing designs similar to those from past years. You may wish to cite them and their results when performing trade studies. However, these design reports are not authoritative, so analysis methods should not be referenced back to them.

2 List of Analysis Tools

1. Trajectory equations, embodied in `451traj.for`. Assumes spherical planet, small flight path angle, etc. Normally set up for earth.

2. Newtonian hypersonic aerodynamics. Sample in `aerodat.for`. Use handouts or your own analysis, to obtain integrals for your vehicle configuration. Define the vehicle axes carefully. Angle of attack is normally zero when the vehicle is nearly symmetric to the flow, when lift is nearly zero.

3. Pitch-plane static-stability analysis, with sample embodied in `aeroprop.for` and `aerotrim.for`. At flight points, $C_m = 0$ (trim), *and* the slope of the C_m vs. α curve must be negative (static stability).

4. Stagnation-point heating equations given in section 7.4 and in Tauber paper. Includes method of approximating TPS temperature. Embodied in `heatflux.for`.

5. Heating analysis for other sample points on vehicle. Equations given in section 7.5. The TPS analysis must be added to this, and coded into `heatflux.for`. For an ablating TPS, the SODDIT code should be used.

6. Skin-friction correlations, see section 7.8. Includes method for estimating boundary-layer transition.

7. Supersonic aerodynamics analysis (Section 7.9).

8. Brief discussion of RCS and life support systems, to be presented later.

9. TPS data from TPSX and other papers to be handed out.

10. Rocket data handout. Detailed data for booster selected.

11. Elementary orbital mechanics, e.g., for pure-propulsive baseline case.

12. Orbital precession data from Bate.

13. Spherical trig. data for orbital crossing angles.

14. Website and structures handouts for structural analysis.

15. Rocket boost analysis using trajectory equations, sample code in `boost.for`. This needs additional development.

16. Cg analysis using Matlab tools from Jason Bowman (see website).

17. Viscous interaction analysis using Lockheed correlation and Boylan paper. If needed, this may be improved upon, using free-molecular flow analysis methods similar to the Newtonian flow analysis methods, and using a bridging formula.

3 Architecture of Framework Programs

Several Fortran-77 programs are provided to you at the AAE450 course directory. These can serve as baseline or framework programs, from which you can develop the code you need to analyze your design. The FORTRAN codes developed by previous students, beginning in Fall 1998, are also provided to you, again on the course directory. These are part of the full design history, which is available. The architecture of the baseline programs is as follows. Most of them were set up to work for Earth, and will need to be modified if used for other planets.

traj.for This is the main program which computes trajectories around a rotating spherical planet. It contains one call to a Microsoft time-and-date routine, which you may have to eliminate or modify to run on the Unix system. It calls:

aerotrim.for This subroutine provides the trimmed aerodynamic parameters for the vehicle – that is, the aerodynamic parameters for flap angles which provide a zero moment that is stable. If no stable flap condition exists for the requested angle of attack, an error flag is returned. It calls:

> **zbrak.for** This Numerical Recipes subroutine is used to help find the value of flap angle β at which the moment is zero (trim). It brackets a region where the moment coefficient passes through zero.

> **zbrent.for** This Numerical Recipes subroutine is used to find the trimmed value of the flap angle. It iterates on `aerodat.for` to find the accurate zero in the moment coefficient.

> **aerodat.for** This function computes the aerodynamic parameters for a vehicle at a given angle of attack and flap angle. You will need to modify this function to represent the hypersonic and supersonic properties of your design. Right now it is programmed to generate data for a flat plate. An earlier version (`aerodat-Gus`) is also available; this earlier version computes aerodynamics for Gus's sample vehicle. The `aerodat` function returns the moment coefficient about the center of gravity (c.g.), which needs to be zeroed for trim. The major part of the semester's aerodynamics work involves generating `aerodat` and `heatflux` subroutines for your vehicle design, and using them to iterate your designs.

trajsub This subroutine contains the equations for the spacecraft dynamics. It calls:

> **heatflux.for** This subroutine computes the heatflux at the stagnation point, and at selected points along the windward surface of the body. This is presently set up for a blunt flat plate. It will also have to be modified to reflect your design.

rk4 This is a Numerical Recipes subroutine to advance the solution of the differential equations by one time step (of 1 sec., usually), using 4th order Runge Kutta.

atmo76 This subroutine supplies the local atmospheric conditions on the earth, given an altitude. A variant is available for Mars.

trajheader.inc This is a file which is included by reference in a number of the subroutines. It defines the number of solution variables used, and the length of the solution arrays. These parameters are defined once in this file so that the parameters are automatically consistent across all the subroutines. For example, when the number of surface temperature solution points is changed, these parameters may need to be changed.

aerotest.for This test program calls `aerotrim.for` for a range of c.g. locations. It can be used with `aeroprop.for` to test `aerotrim.for` to see if the results are ok.

altvmap.for This test program also calls `aerotrim.for`, but for a fixed angle of attack and a range of altitudes and velocities. It can be used to generate data for Tecplot contour plots of L/D, skin friction, and so on.

aeroprop.for This main program generates data for a plot of moment coefficient vs. angle of attack for different flap angles. This plot is used to determine stable trim ranges for a vehicle. This is needed for design purposes. It calls:

aerodat.for See above. The system is structured so this same subroutine can be called by both `aeroprop` and `aerotrim`. Thus you need only generate one version of the aerodynamics.

4   Structural Analysis and Center-of-Gravity Analysis

These are carried out using methods developed by Jason Bowman, AAE451 TA for several years ca. 1996-1998. These methods are documented on the AAE450 website, in considerable detail. Microsoft Word versions of this documentation are also available. A method for determining the loading and required structural weight is given. A simplified finite-element method should be used to compute structural weight, in place of the approximate method used prior to Fall 2001. Also, Matlab software `CGMOI` for computing the combined vehicle center of gravity and moments is given and documented on the website.

   These codes may be written in a language of your choice; however, get the language approved by Prof. Schneider or the TA prior to use, since one of them will need to review your code upon completion.

5   Orbital Dynamics

The orbital dynamics is analyzed using the equations for a point mass vehicle flying above a spherical planet (usually the Earth). These equations are taken from N. Vinh, A. Busemann, and R. Culp, *Hypersonic and Planetary Entry Flight Mechanics*, Univ. of Michigan Press, 1980, Chapter 2. This book is out of print, but a copy of this chapter will be provided to you. In addition, the book is on reserve in the Engineering Library. These equations will be integrated numerically over your trajectory, using a Runge-Kutta or other subroutine. The equations are singular for an orbit that passes precisely over a pole, so latitudes within about 0.1 degrees of the North or South pole must be avoided. The orbital mechanics in this course will be described using Vinh's coordinates.

   The equations described simulate only the 3 spatial degrees of freedom in which the vehicle moves. They do *not* simulate the 3 degrees of freedom associated with vehicle attitude. It will be assumed that the bank angle of the vehicle can be somehow set using the reaction control system (RCS). Section 6.1 describes the requirement for pitch-plane static stability. While this requirement must be met, there is no dynamic simulation of pitch-plane attitude either – it is simply assumed that the vehicle angle of attack can be set as an input. The user thus has arbitrary control over the vehicle angle of attack (within static stability limits), bank angle, thrust (within engine specifications), and thrusting angle (within reasonable limits on nozzle gimballing and the aerodynamics of the vehicle attitude). A more realistic simulation of the vehicle attitude must be left to a more refined design stage.

   Vinh's book is an excellent reference for general orbital trajectory information. For example, once a vehicle has left the atmosphere, it is automatically in an elliptic orbit, assuming the thrust is turned off. One may wish to know the elliptic-orbit properties from the initial state upon atmospheric exit. Section 3.5 of Vinh shows how to compute these elliptic-orbit properties, given such an initial state. Another common issue is the magnitude of the retroburn that should be

carried out to transfer from a circular orbit to a reentry orbit with a particular flight path angle at atmospheric entry. Vinh section 5.4 works out this particular problem.

While the earth will be assumed spherical, nodal regression is substantial for Earth polar orbits. This effect should be accounted for using the empirical data presented in Bate, Mueller, and White, *Fundamentals of Astrodynamics*, Dover, 1971, pp. 156-158.

You will need to use various elements from spherical trigonometry in order to determine the ground track of various orbits, and how to get them to rendezvous. Information for this will be provided in a handout taken from the CRC Standard Math Tables. When two orbits with different inclinations intersect away from the equator, the difference in heading angle must be known in order to compute the pure-propulsive impulse needed to change from one to the other. These relations are given in section 5.2.

There are several references describing trajectory designs for aeroassist. Among these are *Optimal plane change of an elliptic orbit during aerocruise*, by Medepalli and Vinh, AAS Paper 91-417, Aug. 1992.

5.1   Conversion Between Rotating and Inertial Coordinates

The differential equations given in Vinh et al. are written in an Earth-fixed (rotating) coordinate system. If the initial conditions for the differential equations are known in an inertial frame, then they must be converted to the rotating frame before the solution begins. In addition, once the vehicle has left the atmosphere, it is often convenient to perform analyses in the inertial frame (for Hohmann transfers for example).

The following analysis was worked out by Prof. Gustafson to handle this problem. It will be assumed in the following analysis that the flight path angle is a small angle, which would be the case for near-circular orbit, or during most of the reentry trajectory in a planetary atmosphere. We are presently unaware of any reference book containing this analysis.

Consider an initial point at an altitude h and latitude Φ. Then the linear speed of rotation V_s is given by

$$V_s = r\omega, \tag{1}$$

where ω is the angular velocity of rotation of the planet, and r is the radial distance from the axis to the point in question. From Figure 1a, it is seen that

$$\cos \Phi = r / \left(r_e + h \right), \tag{2}$$

where r_e is the radius of the earth. Thus we find that

$$V_s = \omega \left(r_e + h \right) \cos \Phi. \tag{3}$$

In plane H, which is perpendicular to r_e, we must find the relation between the inertial flight velocity V_i and the rotating flight velocity V_e, as well as the relation between the inertial heading angle ψ_i and the rotational heading angle ψ_e. This is done by applying the law of cosines to the triangle shown in Figure 1b, giving

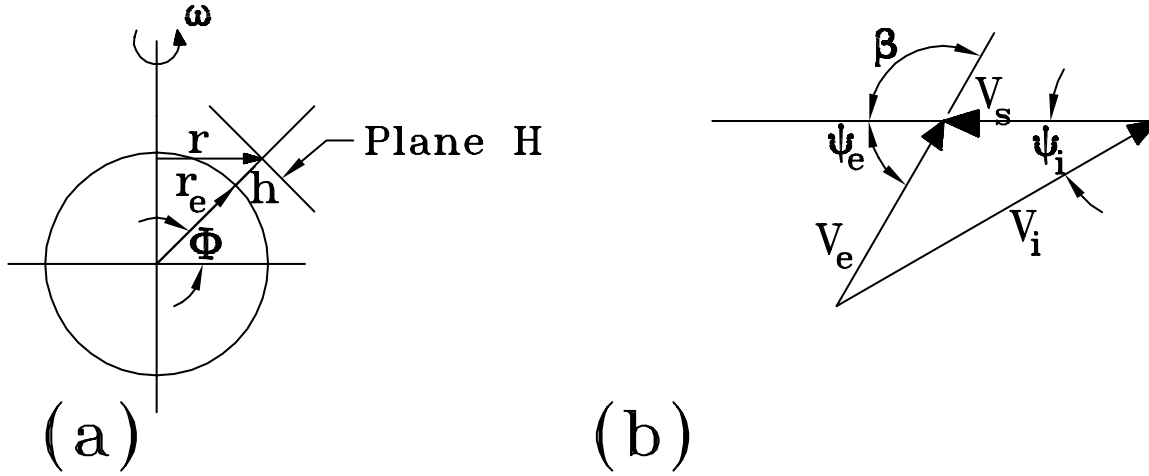$$V_e = \left(V_i^2 + V_s^2 - 2V_i V_s \cos \psi_i \right)^{1/2}. \tag{4}$$

Figure 1: Plane Section of Earth,(a), with Vector Diagram in Plane H,(b)

Applying the law of cosines again allows one to find the angle β as follows:

$$\cos \beta = \left(V_e^2 + V_s^2 - V_i^2 \right) / \left(2 V_e V_s \right). \tag{5}$$

Then $\psi_e = \pi - \beta$, and thus the rotating values of velocity and heading angle are determined in terms of the corresponding inertial values.

The same figures can be used to work backwards from the rotating frame values to the inertial frame values. Using Figure 1b,

$$V_i = \left(V_e^2 + V_s^2 - 2 V_e V_s \cos \beta \right)^{1/2}, \tag{6}$$

where $\beta = \pi - \psi_e$. Again using Figure 1b, we then have

$$\cos \psi_i = \left(V_i^2 + V_s^2 - V_e^2 \right) / \left(2 V_i V_s \right). \tag{7}$$

Note that both of these relations were worked out based on vehicle velocities in quadrant I. For retrograde orbits, a modification of this analysis may be necessary.

5.2 Spherical Trigonometry for Orbits

This section gives a method for computing the differences in heading angle for two planar orbits that intersect away from the equator. See Figure 2, where i_1 and i_2 are the inclination angles for the two orbits, α is the difference between the two heading angles at the interaction point, and θ is the difference between the values of the RAAN for the two orbits.

Use the spherical law of cosines for angles.

$$\cos \alpha = - \cos i_1 \cos \left(\pi - i_2 \right) + \sin i_1 \sin \left(\pi - i_2 \right) \cos \theta, \tag{8}$$

or

$$\cos \alpha = - \cos i_1 (-) \cos i_2 + \sin i_1 \sin i_2 \cos \theta, \tag{9}$$

simplifying to

$$\cos \alpha = \cos i_1 \cos i_2 + \sin i_1 \sin i_2 \cos \theta. \tag{10}$$

For the case of the Space Station and Iridium, the results are plotted in Figure 3.
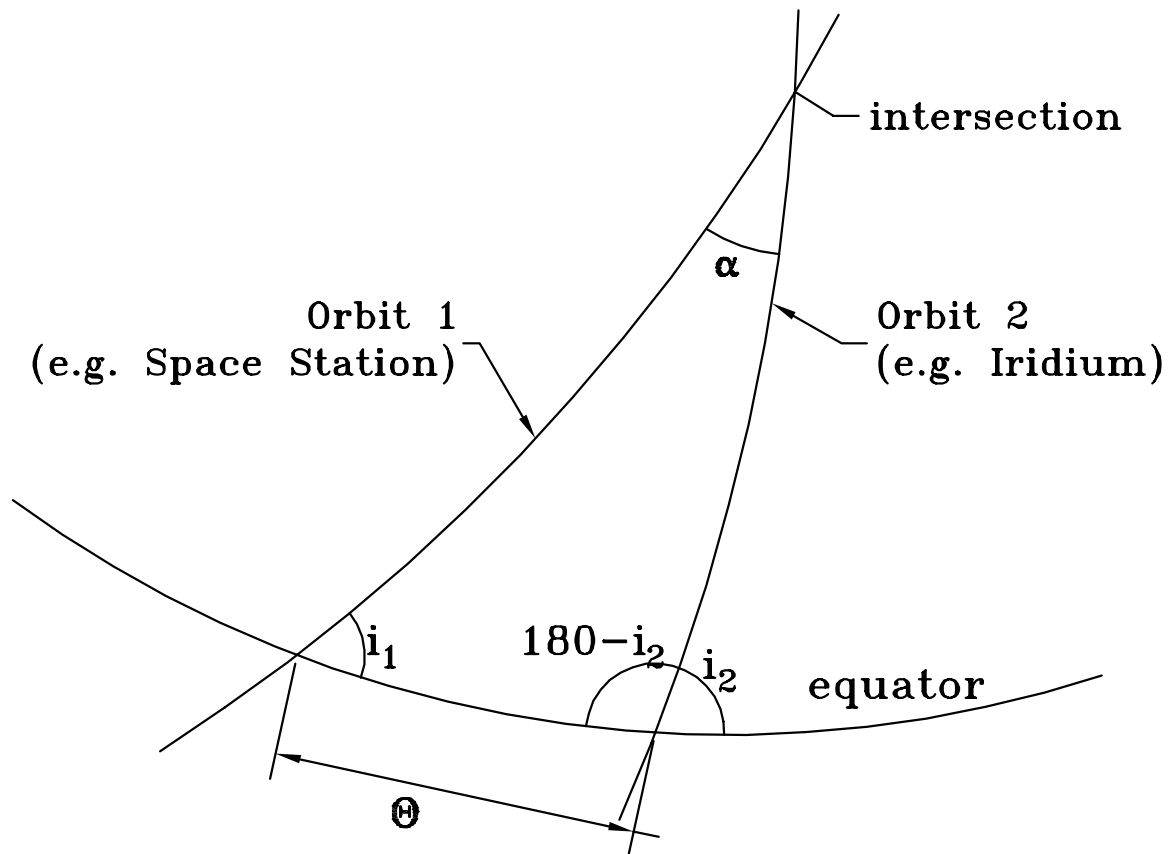
Figure 2: Spherical Trigonometry for Heading Angle Differences

51.6 deg. inclination orbit intersecting a 86.4 deg. orbit whose ascending node is eastward. Angle α is the difference in heading angles at the first intersection above the ascending node. Angle θ is the difference in longitude of the ascending nodes. For θ=0, α = 34.8; for θ = 180, α = 138, the only simple cases.
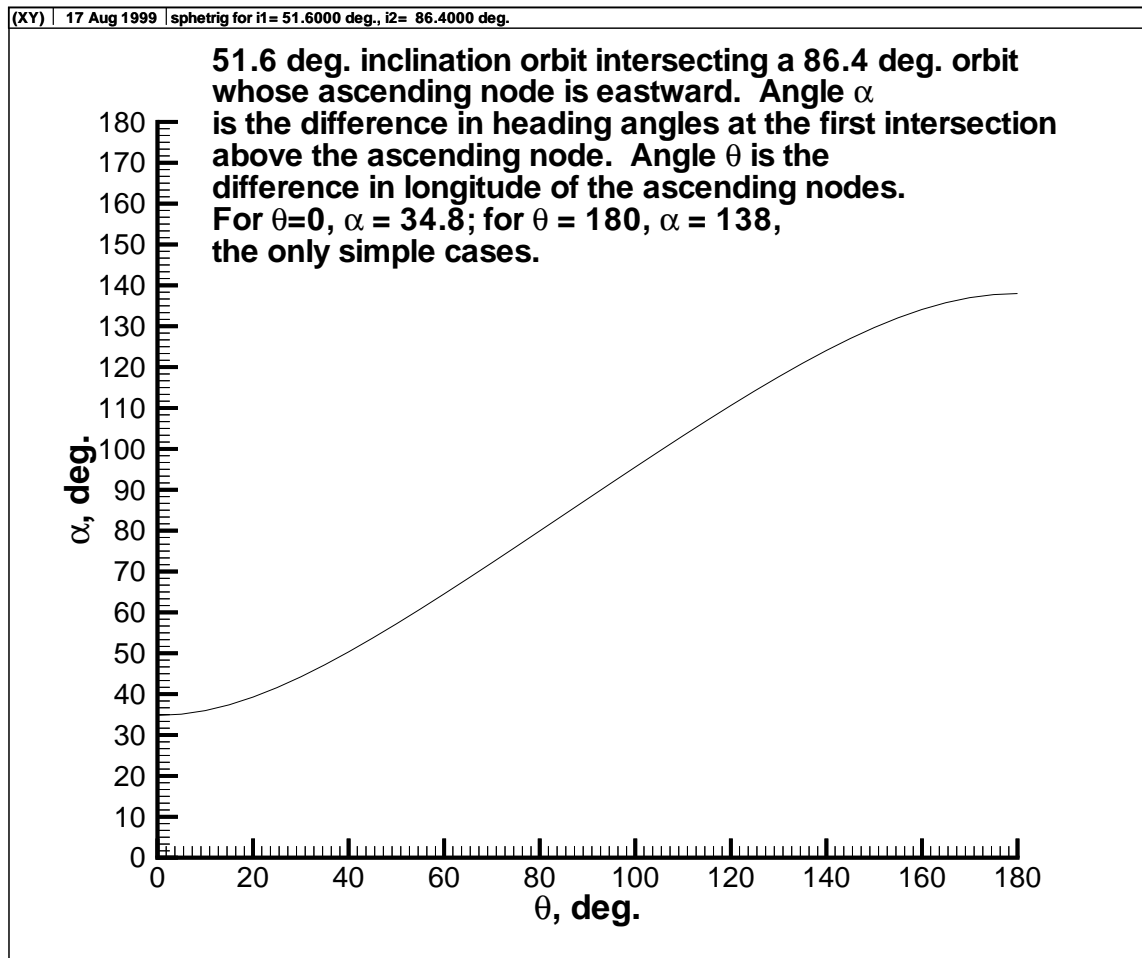
Figure 3: Spherical Trigonometry for Heading Angle Differences
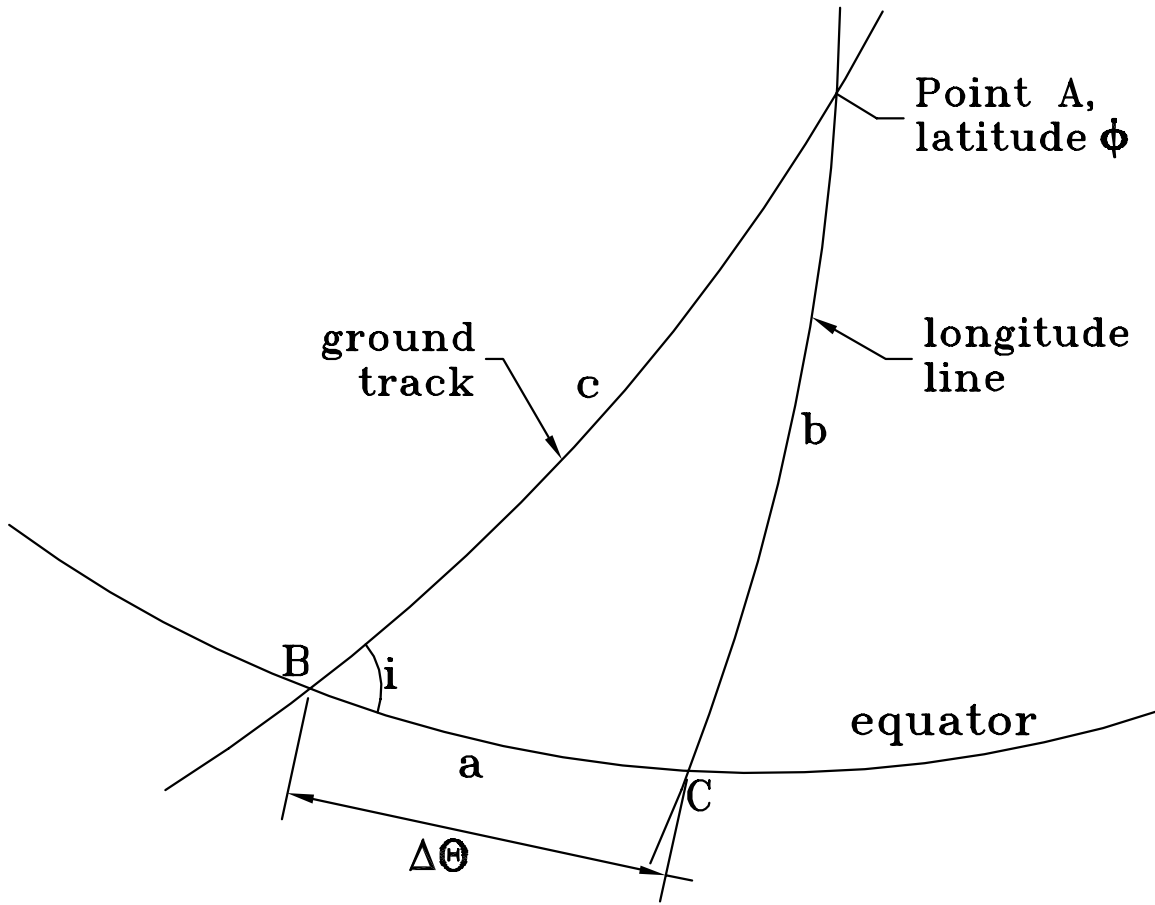
Figure 4: Spherical Trigonometry for Ground Track

5.3 Ground Track and Heading Angle for a Planar Orbit

To keep track of the position of the various orbits, it is often easiest to compute the ground track for them and plot the ground tracks. This requires the use of spherical trigonometry; see, for example, the CRC Standard Math Tables. Figure 4 shows the geometry. Note that there is a spherical right angle at point C. Here, however, we will use the general formulas for oblique spherical triangles.

From the law of sines,

$$\frac{\sin a}{\sin A} = \frac{\sin b}{\sin B},$$

(11)

where A is the angle at point A, a is the length of the opposite side, and so on. This implies that

$$\frac{\sin \Delta\theta}{\sin A} = \frac{\sin \phi}{\sin i},$$

(12)

where i is the inclination angle, and

$$\sin A = \frac{\sin \Delta\theta \sin i}{\sin \phi}.$$

(13)

From the law of cosines,

$$\cos B = -\cos C \cos A + \sin C \sin A \cos b, \tag{14}$$

so

$$\cos i = -\cos\left(\pi/2\right)\cos A + \sin\left(\pi/2\right)\sin A \cos\phi, \tag{15}$$

where $\cos\left(\pi/2\right) = 0$ and $\sin\left(\pi/2\right) = 1$. Therefore,

$$\cos i = \sin A \cos\phi. \tag{16}$$

Using equation 13, we then have

$$\cos i = \frac{\cos\phi}{\sin\phi}\sin\Delta\theta\sin i, \tag{17}$$

or

$$\cot i = \cot\phi\sin\Delta\theta. \tag{18}$$

Note that $\Delta\theta$ is the longitude measured from the Right Ascension of the Ascending Node (RAAN), point B. This can be rewritten as

$$\tan\phi = \tan i \sin\Delta\theta, \tag{19}$$

where $\tan i$ is a nonzero constant. Simplifying,

$$\phi = \arctan\left(\tan i \sin\Delta\theta\right). \tag{20}$$

Note that this does NOT account for the rotation of the earth, as it is derived in inertial space. Using Bate p. 142, we have that

$$\cos i = \sin\left(\pi/2 - \psi\right)\cos\phi, \tag{21}$$

or

$$\cos i = \cos\psi\cos\phi. \tag{22}$$

This gives the inclination angle i in terms of the heading angle ψ and the latitude ϕ. Also, using Fig. 2.15-2 in Bate, and the fact that the angle $B = \pi/2$, and the law of cosines, we have that

$$\cos\left(\pi/2 - \psi\right) = -\cos i \cos\left(\pi/2\right) + \sin i \sin\left(\pi/2\right)\cos\Delta\theta, \tag{23}$$

so

$$\sin\psi = \sin i \cos\Delta\theta, \tag{24}$$

and

$$\cos\Delta\theta = \frac{\sin\psi}{\sin i}. \tag{25}$$

This gives the angle $\Delta\theta$ between the local longitude and the RAAN, given i and ψ.

Figure 5 shows the computed results for the space station orbit plane. Note the difference from the intuitive formula which one might incorrectly guess.
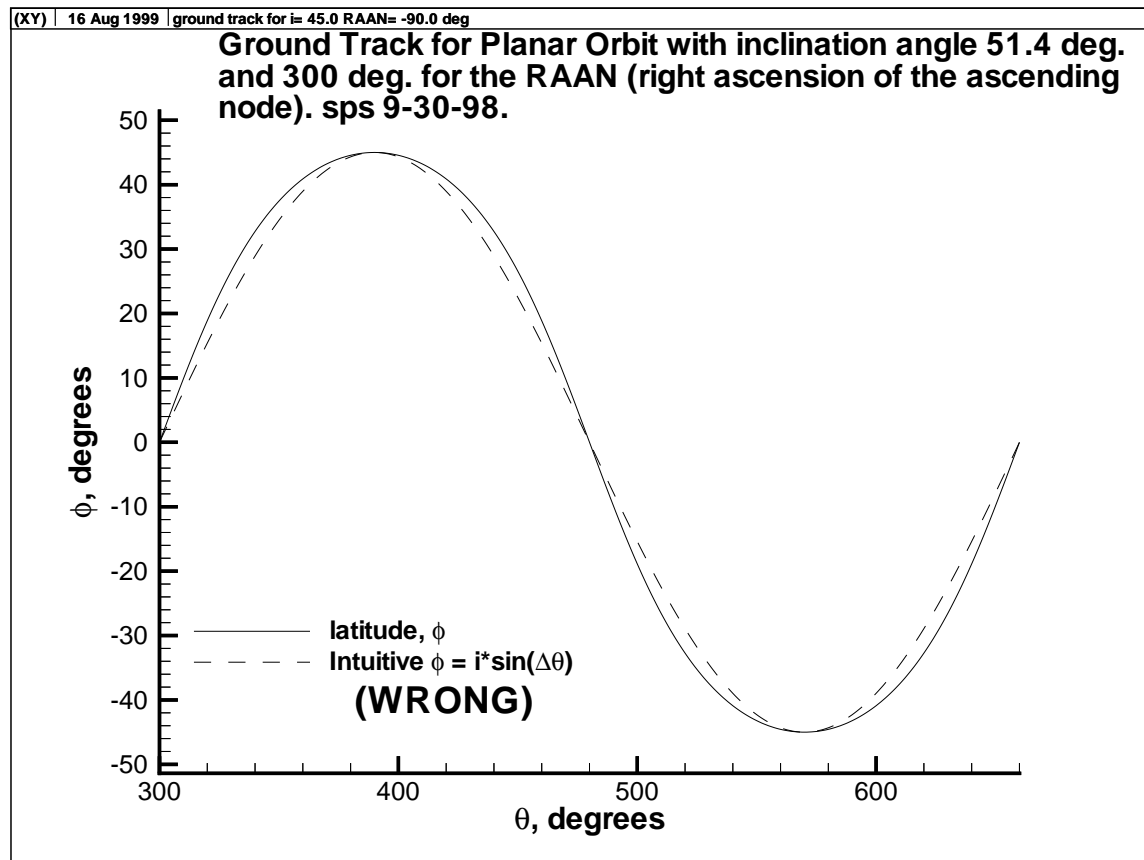
Figure 5: Ground Track for Space Station Orbit

5.4 Single-Point Cruise Design

Here, consider a single point cruise design for an aeroassist mission, in order to have a relatively simple basis to trade altitude, wing loading, and so on.

5.4.1 Inclination Angle Changes

Consider a single point cruise design, carried out at the equator, for a small time Δt. The vehicle is at point B in Figure 4. Look at a tangent plane near B. We have velocity V at inclination i, and want to change to velocity V_2 at inclination $i + \Delta i$. The velocity and altitude are assumed constant, and heating should be considered separately. Figure 6 shows the geometry. We want
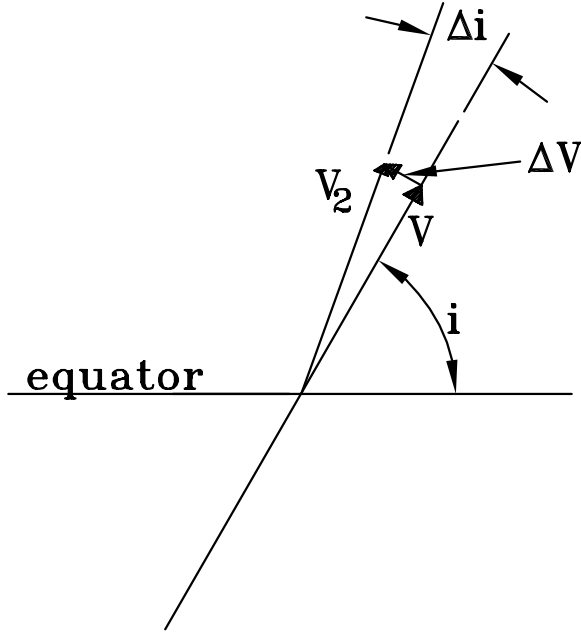
Figure 6: Inclination Angle Change for Single Point Cruise Design

to change from a velocity V at inclination i to a velocity V_2 at inclination $i + \Delta i$. For small Δi, the same law of cosines used earlier gives

$$\Delta i = \Delta V / V. \tag{26}$$

Consider a vehicle at bank angle σ; the component of the lift in the vertical plane is then $L \cos \sigma$ while the component in the horizontal plane is $L \sin \sigma$. For a small time Δt, $\Delta V = a \Delta t$, where a is the acceleration in the horizontal plane, $L \sin \sigma / m$, where m is the vehicle mass. Thus,

$$\Delta V = L \sin \sigma \Delta t / m, \tag{27}$$

or

$$\Delta i_{syn} = L \sin \sigma \Delta t / (mV). \tag{28}$$

This same equation can be obtained from the third part of equation (2-31) in Vinh's book, by looking at the equator, where heading angle equals inclination angle, latitude is zero, and flight path angle is zero.

Constant horizontal velocity is maintained by holding thrust T equal to drag D. The single-point design condition also assumes we have enough vertical force at this bank angle to maintain constant altitude, which requires

$$L \cos \sigma = m \left(g - V^2/R \right), \tag{29}$$

where R is the height above the center of the earth, $g = \mu_g/R^2$ is the local gravitational acceleration, and this last term is the centripetal acceleration. Outside the atmosphere, $L = 0$, and the two right-hand terms balance to make a circular orbit, with the usual velocity $V_{orb} = \sqrt{\mu_g/R}$. Here, μ_g is the gravitational constant for the planet, and should not be confused with the viscosity.

Equation (29) can be obtained from the second part of equation (2-31) in Vinh's book, again looking at the equator, with zero latitude and flight path angle. However, in this case we need to add some terms that come about from the rotating earth (angular velocity ω):

$$0 = (L/m) \cos \sigma - g + V^2/R + 2\omega V \cos i + \omega^2 R \tag{30}$$

The $2\omega V$ term is the Coriolis acceleration, according to Vinh, and may be important for long-range flight. The $\omega^2 R$ term can usually be neglected, according to Vinh. Here, we will neglect both of these terms for an initial cruise-point analysis.

For a maneuver done with pure propulsion, outside the atmosphere, the same ΔV is needed. For a small time Δt, $\Delta V = a\Delta t$, still, where a is again the acceleration in the horizontal plane, which is now the thrust of the rocket. If we use the same thrust for the same length of time, we will use the same amount of fuel, and achieve

$$\Delta V_{pp} = (D/m)\, \Delta t. \tag{31}$$

Thus,

$$\Delta i_{pp} = D\Delta t / (mV). \tag{32}$$

Taking the ratio, we have

$$\frac{\Delta i_{syn}}{\Delta i_{pp}} = (L/D) \sin \sigma. \tag{33}$$

This is the best case for efficiency. Efficiency will be reduced due to viscous interaction during entry and exit, due to operation away from the equator where bank affects not only i but also the RAAN, and other effects. Ideally, the maneuver can be carried out in a short distance near the equator, and entry and exit can be a small portion of the maneuver. If V is maintained near orbital speed, σ can be near 90 degrees, and the efficiency can approach L/D, making an aeroassist vehicle useful and practical.

5.4.2 Altitude Effects

To maintain the cruise altitude, we require thrust equal to drag. This requires

$$T = \frac{1}{2}\rho V^2 A C_D, \tag{34}$$

where T is thrust, and A is the reference area for the C_D computation. We can also write equation (29) in terms of the lift coefficient,

$$\frac{1}{2}\rho V^2 A C_L \cos\sigma = m\left(g - V^2/R\right).\tag{35}$$

The lower the altitude, the higher ρ is. This increases both L and D in the same proportion. Note that

$$T(L/D)\cos\sigma = m\left(g - V^2/R\right).\tag{36}$$

For a given L/D ratio, the allowable bank angle σ increases with maximum thrust and with cruise velocity. If we normalize this equation, we get

$$(T/mg)(L/D)\cos\sigma = 1 - V^2/(gR),\tag{37}$$

or

$$(T/mg)(L/D)\cos\sigma = 1 - RV^2/\mu_g,\tag{38}$$

or

$$(T/mg)(L/D)\cos\sigma = 1 - V^2/(\mu_g/R),\tag{39}$$

or

$$(T/mg)(L/D)\cos\sigma = 1 - (V/V_{orb})^2.\tag{40}$$

If $V = V_{orb}$, then a 90-deg. bank angle can be maintained independent of $T/(mg)$ and L/D. For smaller V, these two parameters must increase to allow the constant-condition cruise.

At lower altitudes, heating is greater, which will require a heavier thermal protection system (TPS, see Section 7). Clearly, the altitude should be low enough to minimize viscous-interaction drag (Section 7.10), in order to obtain maximum L/D. Heating is then the dominant concern – can V be maintained near V_{orb} without excessive heating? Otherwise, it may be desirable to decrease V in order to reduce heating, while increasing $T/(mg)$ in order to be able to maintain the altitude and high bank angle.

Note that the viscous interaction parameter $VI = M_\infty/\sqrt{(Re_\infty)}$. Approximate that the sound speed is fairly independent of altitude. Then VI is proportional to $\sqrt{V/\rho}$. From equation (46), the heat transfer seems approximately proportional to $\rho^{0.5}V^3$.

5.5   Reentry Trajectories

See Vinh for a discussion of these. Chapter 5 covers methods of computing the retroburn ΔV to achieve a given flight path angle at atmospheric interface (γ_e.) Using these techniques, or trial and error, one would normally try to obtain $-1.5 > \gamma_e > -3$ degrees. An angle of -5 to -6 degrees may be too steep, and will often cause excessive heating. A lifting vehicle lets the trajectory person control the heating. Typically the altitude oscillates during reentry if the angle of attack and bank angle are not modulated. If the wing area is too small, the vehicle will sink too fast. The wing area, or lift to mass ratio, is a critical parameter. Gus's sample vehicle has too small of a wing area. Typically one runs some trajectories and tries out some modulation algorithms, and evolves the design using trial and error. For a shuttle-like vehicle, one usually holds a bank angle

of roughly 45 deg., and then reduces it at some point to increase lift. The shuttle has used bank angles to 60-65 deg. at times. It is necessary to compute the footprint of where you can land from a given deorbit location – what is the down and cross-range? Where can you land?

To get crossrange, it is usual to run a zero-bank trajectory to get the nominal conditions, and then run the banked trajectory to get the crossrange. The crossrange is the distance along the surface of the earth, in the direction normal to the zero-bank trajectory.

Note that the engine nozzles should not be exposed to the reentry flow. The shuttle has fairings to preclude this.

6 Stability and Control

6.1 Vehicle Attitude Control

The stability and control methods used in the course are limited to requiring static stability in the pitch plane during hypersonic flight. The static stability issues are discussed in H. Ashley, *Engineering Analysis of Flight Vehicles*, Dover, 1992, pp. 247-248. You must 'fly' your vehicle in a trimmed state, with $C_m = 0$, where C_m is the pitching moment coefficient. To accomplish this, some kind of flap control is needed. In addition, you must demonstrate static stability, that is $dC_m/d\alpha < 0$, where α is the angle of attack. The amount of margin that is required does not seem to be a clearcut issue. Penland (1978) calls for $dC_m/dC_L < X$, where X is at least 0.02. Penland notes that *'a value of $dC_m/dC_L = -0.02$ indicates that the lift vector is located 2% of the fuselage length behind or downstream of the moment reference or c.g. of the airplane and the vehicle is said to possess a static margin of 2%.'*. For Penland's vehicle, where this is 4% of the wing chord, the static margin is said to be *'minimal but adequate'* (Penland 1978 p. 6).

These simple requirements cause critical interactions between the various design components and make the design truly multidisciplinary. For example, a change in the location of the propellant tanks for the propulsion system will cause a change in the center of gravity, which will thus cause a change in C_m. Due to fuel usage, C_m and the associated aerodynamics and stability may change during your trajectories, and this needs to be monitored. An example of a static-stability diagram is shown in Fig. 7 for the blunt flat plate that is discussed in Section 7.11.

6.2 Design of Controllers for Trajectories

In several cases, it is desirable to control the vehicle so as to reach a target altitude or trajectory. For example, it may be desirable to reach a target cruise altitude during an aeroassist maneuver, without excessive overshoot oscillations, by appropriate control of the bank angle as a function of time. How should the bank angle be set so as to achieve this goal? Control theory can be used to help with this part of the design (see, for example, the reference by Franklin et al.).

Much of introductory control theory is limited to the case of a linear system with a known transfer function (see, for example, the appendix of the AE421L notes, by Prof. Rotea). The equations of motion for the vehicle are nonlinear. Although a local linearization could be carried out for specific locations, the effort involved is probably prohibitive for this course.

However, PID control can still be used, as suggested by Rotea and as discussed in Appendix A.3 of the 421L notes. The controller should not be connected until the vehicle is reasonably close
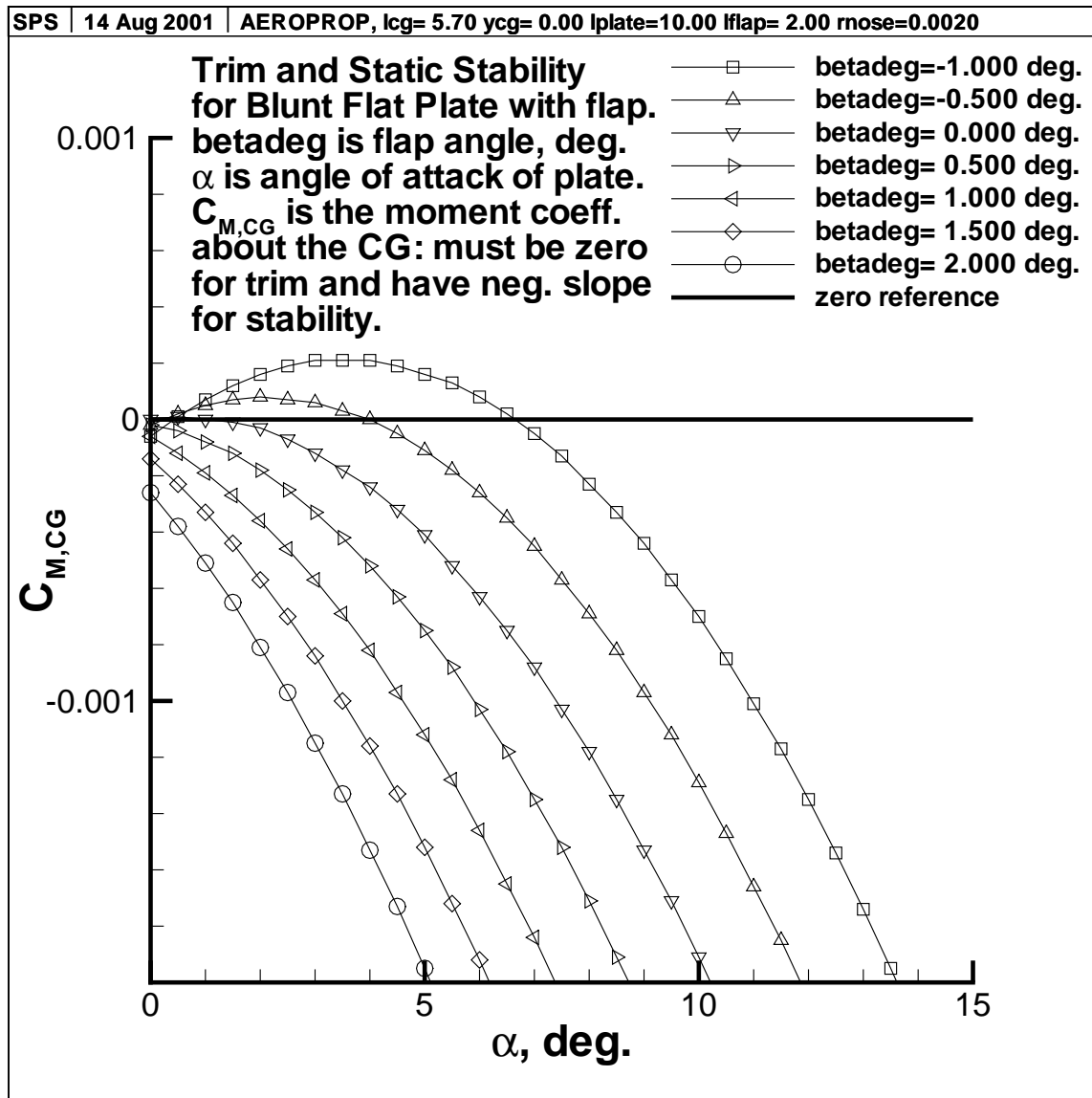
Figure 7: Sample Trim Plot for Blunt Flat Plate with Flap

to the target trajectory. In the cruise altitude example, the controller turn-on altitude would be another design parameter. The control law in the time domain is

$$u(t) = k_p e(t) + k_d \dot{e}(t) + k_i \int_0^t e(\tau) d\tau, \tag{41}$$

where $u(t)$ is the control signal, $e(t)$ is the error signal, and k_p, k_d, and k_i are the gains associated with each component of the controller – proportional, derivative, and integral. In the example of the target cruise altitude, $e(t) = h_0 - h$ would be the difference between the current altitude, h, and the target altitude, h_0, and $u(t)$ would be the bank angle. Rotea suggests setting $k_i = 0$, at least initially. If steady-state errors occur when $k_i = 0$, then increasing k_i should solve this problem, although large k_i can destabilize a system. Of the two remaining gains, k_d controls the extent and amplitude of the oscillations, and k_p controls their frequency. These parameters can be used in a trial-and-error study to obtain sufficient control. Rotea suggests starting with $k_p = k_d = 0$, and slowly increasing the two, one at a time, starting with k_p.

It is critical to keep close track of the signs of the feedback parameters, which must be such as to provide damping and a restoring force, when examined using a mass-spring-damper analogy. In this analogy, one notices that $u(t)$ provides a restoring force, so that $u = mc_1 \ddot{h}$, where m is the vehicle mass and c_1 is some 'constant' (which is actually a constant only in a linear system). It is immediately apparent that the system is analogous to the mass-spring-damper system.

In the cruise-altitude example, Rotea suggests

$$u(t) = k_p (h_0 - h(t)) - k_d \dot{h}(t), \tag{42}$$

where $k_p > 0$ and $k_d > 0$. Here, we assume increasing $u > 0$ increases the force that tends to increase h; otherwise, change the sign of k_d. Be wary of including feedback on an $\dot{h}_0(t)$ term in the controller (of changing the target altitude within the controller), since this can cause instability.

In the target cruise altitude example, a number of trajectories could be simulated, with increasing values of the gains, until a suitable trajectory is obtained. The properties of the PID controller will be discovered through this process. In particular, it will be found that it is impossible to reach and remain at the target altitude with $k_d = 0$, using only information about the current altitude – the vehicle will simply oscillate about the target altitude. To achieve the target altitude without large oscillations, it is essential to include information about the rate of change of the altitude. This information provides the damping term, in the mass-spring-damper analogy.

In some cases small high-frequency oscillations may remain, particularly in the bank angle (or other control parameter). These can be removed by low-pass filtering the bank angle (or other parameter, such as the rate of change of altitude). This is done by adding a differential equation to the system. For example, if $\dot{h}$ is the rate of change of altitude, we can create a new parameter $y = \dot{h}_f$, where $\dot{h}_f$ is the filtered rate of altitude change. One then determines y by solving

$$T_f \dot{y} + y = \dot{h}, \tag{43}$$

simultaneously with the other equations. Begin with a small amount of filtering by using a very small value for the parameter T_f. Note that if $T_f = 0$ the original system is recovered. Since excessive filtering can make the system unstable, proceed cautiously. Consult Prof. Rotea for further suggestions.
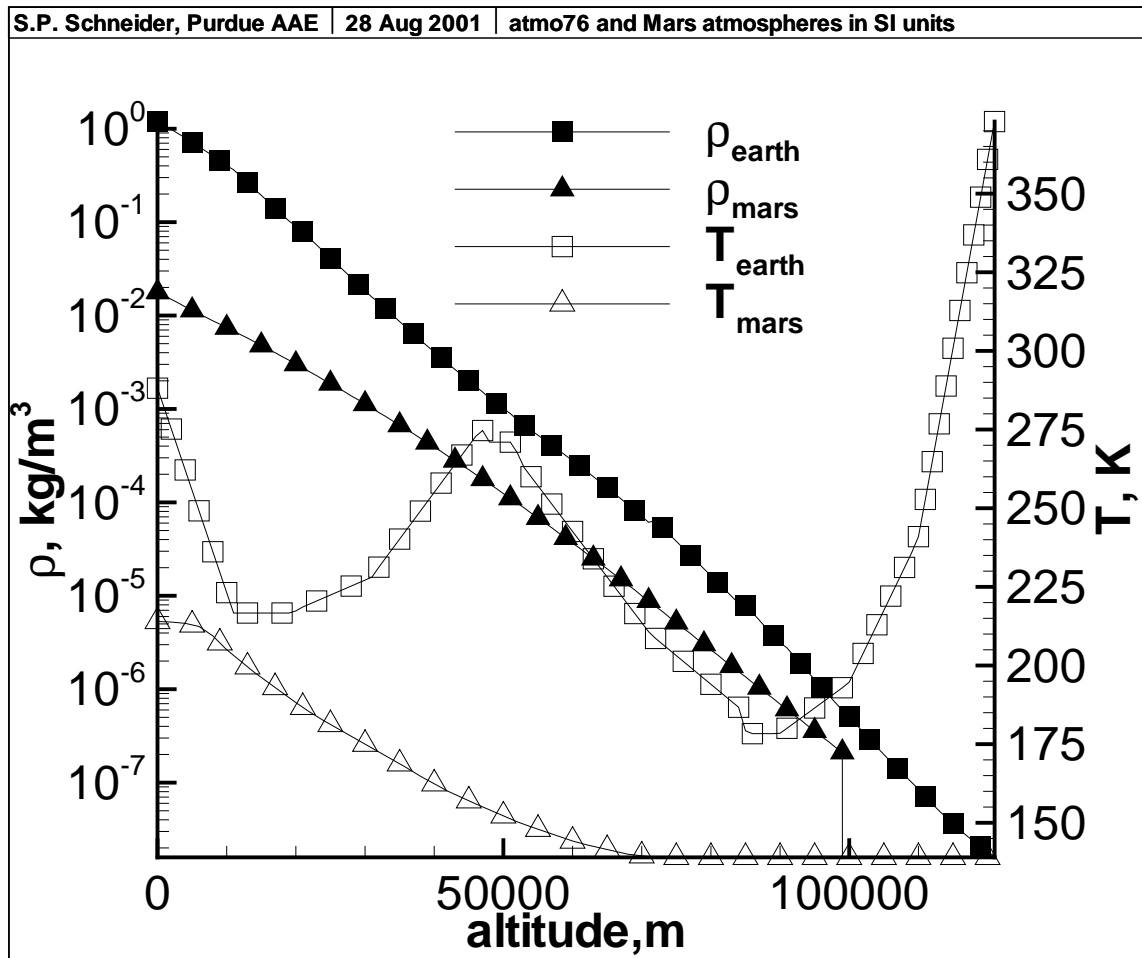
Figure 8: Properties of Atmospheres of Earth and Mars

7   Aerothermodynamics

Simplified aerodynamics are also used, to allow multidisciplinary design iterations. The vehicle shape is generated by adding together simple shapes, like cones and cone frustra, flat plates, spherical sections, and so on. A more sophisticated surface panel method of defining the geometry would be too complex to allow multidisciplinary iteration during the time available for the course.

7.1   Atmospheric Conditions

For earth, these are taken from the 1976 Standard Atmosphere, as coded by Prof. Gustafson, and checked against tables (e.g. *Handbook of Tables for Applied Engineering Sciences*, Bolz and Tuve, CRC Press). For Mars and Venus, atmospheric data can be taken from the references in Seiff, *Atmospheres of Earth, Mars, and Venus, as Defined by Entry Probe Experiments*, J. Spacecraft and Rockets, v. 28, no. 3, pp. 265-275, May-June 1991. A *FORTRAN* program has been written to generate the properties of the Mars atmosphere. Figure 8 shows the exponential decrease of density with altitude.

Figure 9: 2D Wedge for Newtonian Flow Analysis

7.2 Pressure

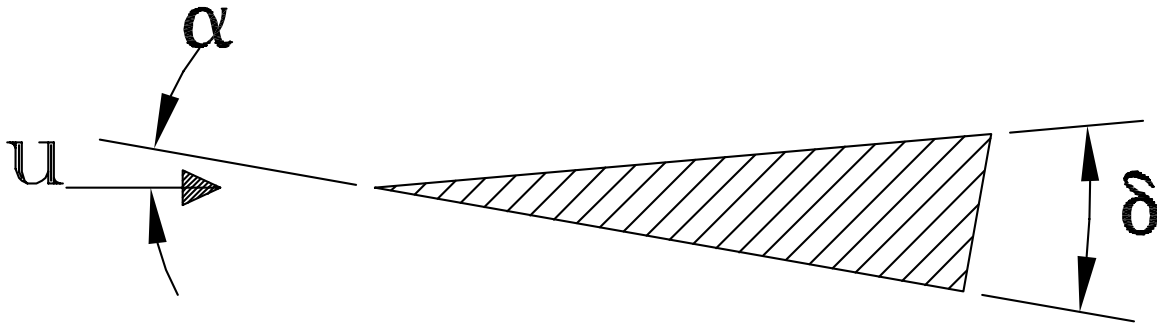The aerodynamic pressure on the vehicle surfaces is evaluated using Newtonian methods. These are described, for example, in J. Anderson, *Hypersonic and High-Temperature Gasdynamics*, AIAA Publications, 1989, Chapter 3. The Newtonian pressures have been integrated over simple shapes by E. L. Clark and L. L. Trimmer, *Equations and Charts for the Evaluation of the Hypersonic Aerodynamic Characteristics of Lifting Configurations by the Newtonian Theory*, AEDC-TDR-64-25, March 1964. A copy of this report will be provided to each group. Clark's results allow you to proceed directly to coding the analytical results for the various simple shapes which your vehicle will be a composite of. Be careful to note, however, that Clark's results are given in the frame of reference of the vehicle (axial and normal force), and need to be translated to the frame of reference of the velocity vector (lift and drag). This step was omitted by most of the Fall 1998 groups, causing errors of unknown magnitude in their results. You must also make appropriate allowances for shadowing effects.

Pitching-moment coefficients should be computed based on the inviscid Newtonian aerodynamics. While the skin friction will also contribute to the pitching moment, it has a smaller effect. Therefore, to save the non-trivial effort of taking them into account, skin-friction effects on pitching moment should normally be neglected. Rarefied-flow viscous interaction will also have an effect on the pitching moments (see Section 7.10); however, this effect is difficult to predict, so again it will have to be neglected.

7.3 Wedge Aerodynamics: Some Design Issues

For an aeroassist orbital transfer vehicle, a high lift-to-drag ratio is clearly critical (cp. Section 5.4). The following is a first look at the issues involved, for a vehicle with small nose bluntness. The material is adapted from the work of Shin Matsumura, AAE451, Fall 1999, LEOTARD group.

Anderson works out the lift and drag of a flat plate as part of his discussion in section 3.2 of HHTG. In Fig. 3.6, he shows that the lift-to-drag ratio, L/D, becomes very large for small angles of attack (small α). Since the hypersonic Newtonian pressure depends only on local incidence angle, it would seem that the flat plate at small α has the best possible L/D. Of course, a flat plate has zero internal volume for cargo; however, a wedge with a top face that is parallel to the flow has the same Newtonian aerodynamics as a flat plate. Fig. 9 shows the geometry. Here, δ is the included angle of the wedge. Note that α is defined with respect to the lower surface of the

wedge.

The Newtonian lift and drag coefficients for a flat plate are given by Anderson on p. 51 of HHGD. These were coded into `wedgeaero.for`, taking into account both upper and lower surfaces, along with the shadowing effect. The resulting L/D is shown in Fig. 10. Of course, the flat plate
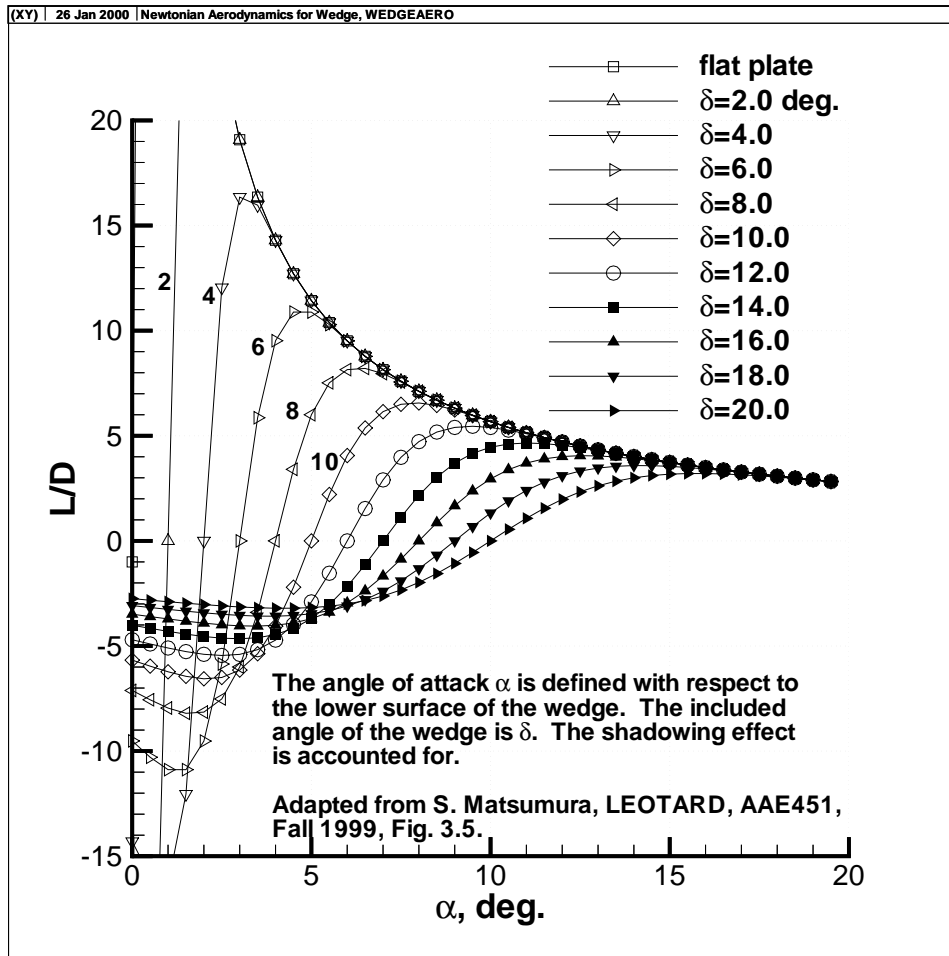
Figure 10: Newtonian Lift-to-Drag Ratio for 2D Wedge

has the best L/D. Anderson shows that the Newtonian L/D goes like $\cot\alpha$ and becomes infinite as $\alpha \to 0$. Of course, this neglects skin friction, etc. For $\alpha < \delta/2$, L/D is negative, since $L < 0$. As angle of attack increases for a particular δ, L/D rises until the upper surface is shadowed (at $\alpha = \delta$), after which L/D is the same as for a flat plate. For smaller δ, the upper surface becomes shadowed for smaller α, where L/D is larger. For example, for an included angle of $\delta = 6$ deg., $L/D > 10$ is possible. This is a best-case limit, since skin friction, nose bluntness, trim drag, and viscous interaction will reduce L/D. However, it points to the classically critical importance of a slender vehicle. Like the Carnot efficiency in thermodynamics, this simple analysis shows a best possible case.

These high values of L/D at low α come at a price. Fig. 11 shows the lift coefficients for these same shapes. Again, the flat plate is the best case. The wedges have lesser or negative lift coefficient, until the upper surface is shadowed, after which they match the flat plate. Note

Figure 11: Newtonian Lift Coefficient for 2D Wedge

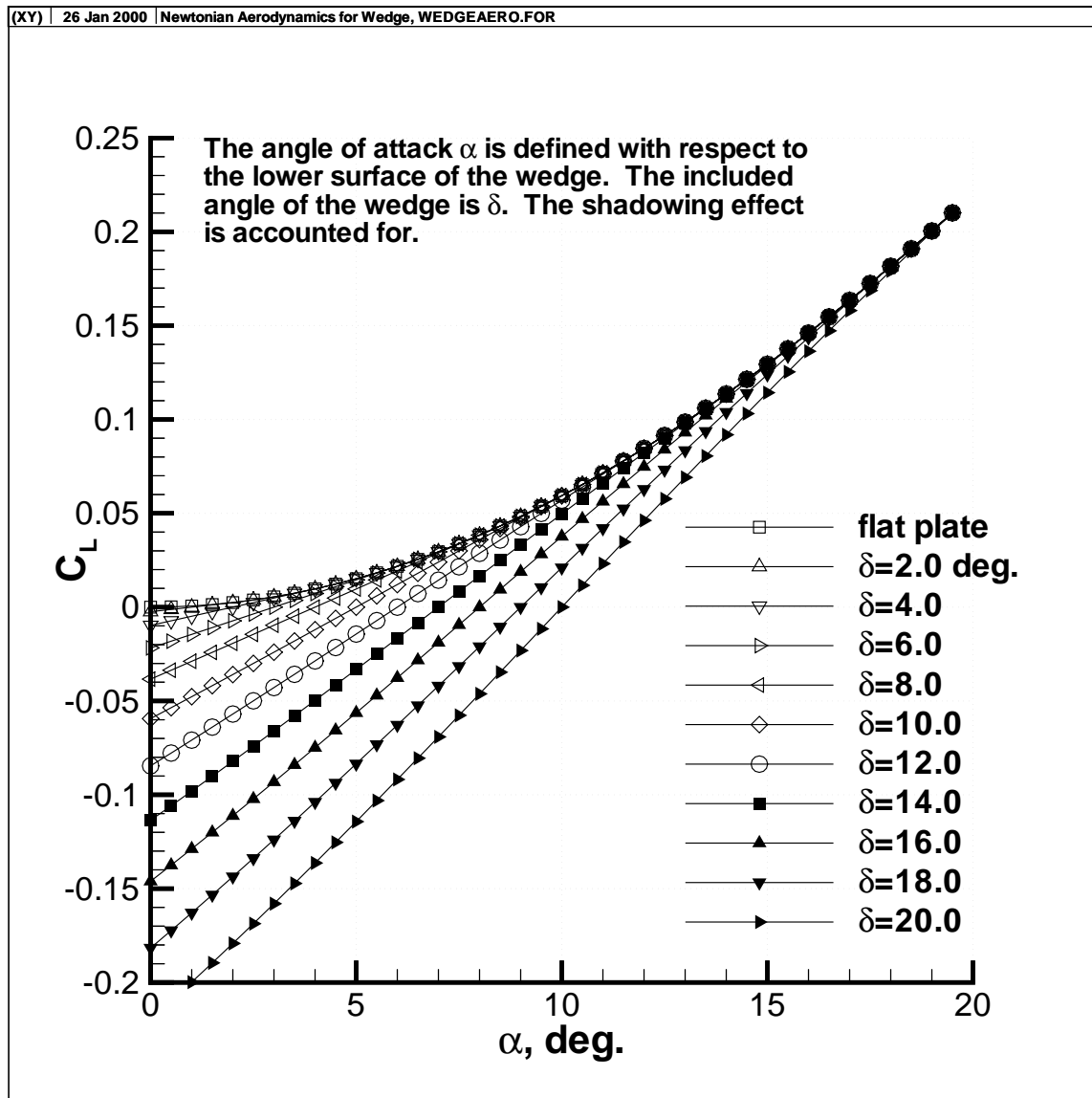how small C_L is: at $\alpha = 5$ deg., where a 6-deg. wedge has $L/D \simeq 11$, $C_L = 0.0015$. Although $q = 0.5\rho V^2$ is typically very large for a hypersonic vehicle, these small lift coefficients may make lift-to-weight ratio a critical issue, depending on altitude, density, and velocity.

Of course, the drag coefficients are much smaller still, for small α, as shown in Fig. 12. Here, we see high drag until the upper wedge surface is shadowed, after which the flat plate value is matched. A slender wedge is required to shadow the upper surface at angles of attack where a high L/D is possible. This slender wedge may create problems with internal volume, although these can be alleviated by increasing the vehicle length. It is really the skin friction which will limit the slenderness used. Increased slenderness means a longer vehicle and more surface area for the same internal volume; at some point, skin friction will dominate (see design papers by W. Hankey).

7.4   Stagnation-Point Heating Analysis

The following contains the critical elements of the stagnation-point heating analysis for Earth reentry, as adapted from Prof. Gustafson's notes. Note that simplified methods for estimating heat transfer are also given in Hankey, *Reentry Aerodynamics*, AIAA Education Series, 1988. The primary purpose of the heating analysis is to enable designing the thermal protection system (TPS), which must protect the vehicle from the high temperatures of planetary entry.

7.4.1   Stagnation-Point Heat-Transfer Rate, Earth

This is taken from Tauber, Menees and Adelman, *Aerodynamics of Transatmospheric Vehicles*, J. Aircraft, v. 24, n. 9, Sept. 1987, pp. 594-602 (see also Anderson, HHTG, p. 291, eq. 6.169). Equation (4) gives the heating rate per unit area as

$$\dot{q} = C\rho^N V^M. \tag{44}$$

Here, $\dot{q}$ is the heat-transfer rate into the body, per unit area, ρ is the freestream density, and V is the flight velocity. Note that despite the use of $\dot{q}$ for heat transfer, following Tauber et al., no time derivatives are involved, and the plain symbol q is used for the same quantity in most references. The appendix of this paper gives the constants, for a fully catalytic surface (a conservative approximation). The constants give the heating rate in W/cm^2 if the velocity is given in m/s and the density in kg/m^3. The constants are $M = 3, N = 0.5$, and

$$C = (1.83 \times 10^{-8})r_n^{-1/2}(1 - g_w), \tag{45}$$

where r_n is the body nose radius, in meters, and g_w is the ratio of wall enthalpy (h_w) to total enthalpy (h_0). From thermodynamics, $h_w = c_{pw}T_w$. The total enthalpy is $h_0 = h_a + 0.5V^2$, where h_a is the local enthalpy of the atmosphere. However, for reentry h_a is usually much smaller than $0.5V^2$, and will be neglected. This results in

$$\dot{q} = 1.83 \times 10^{-8}\left[\frac{\rho}{r_n}\right]^{0.5}V^3(1 - \frac{c_{pw}T_w}{0.5V^2}). \tag{46}$$
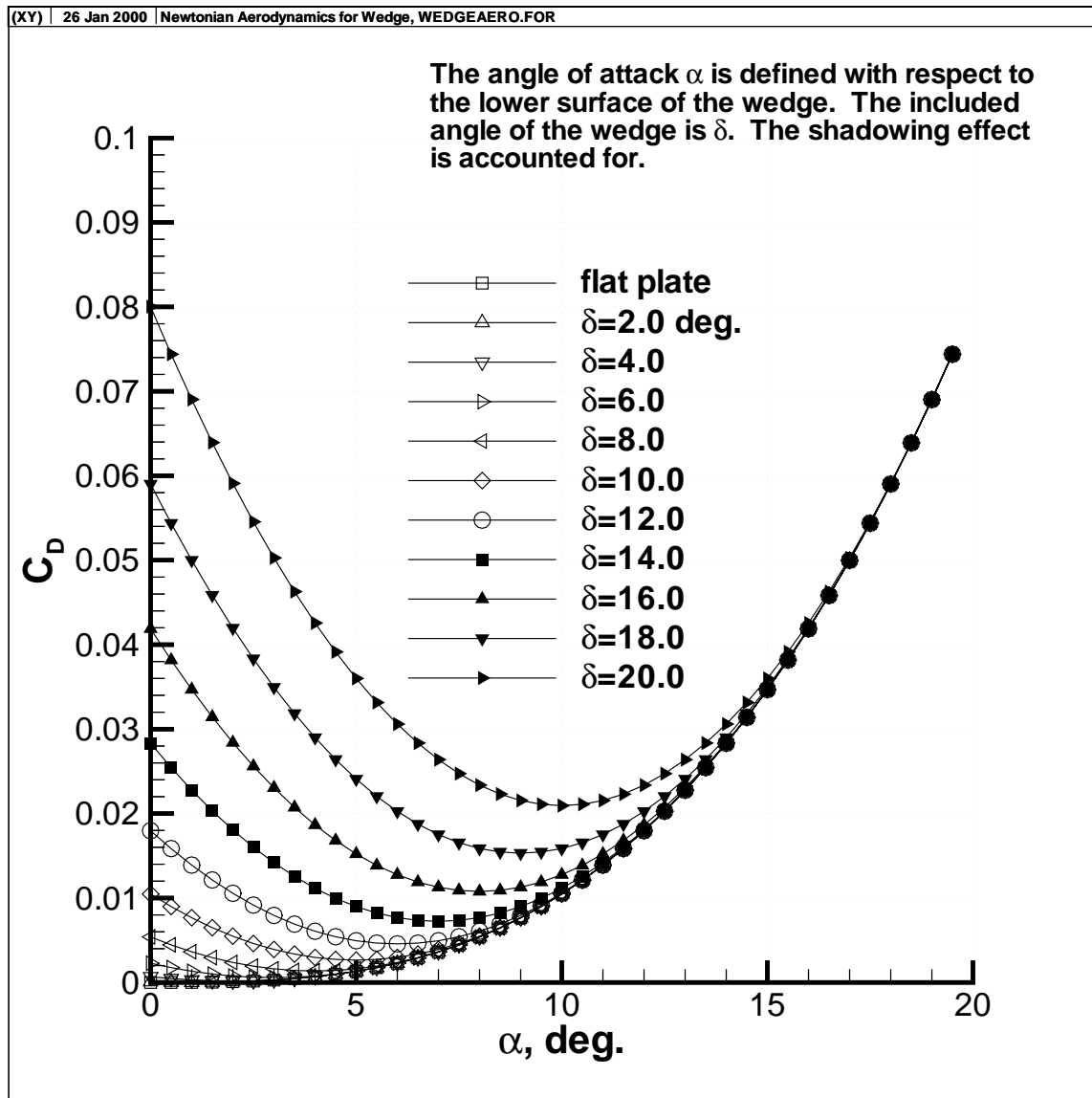
Figure 12: Newtonian Drag Coefficient for 2D Wedge

7.4.2 Stagnation-Point Heat-Transfer Rate, Mars

This can be taken from Tauber and Sutton, *Stagnation-Point Radiative Heating Relations for Earth and Mars Entries*, J. Spacecraft and Rockets, v. 28, no. 1, pp. 40-42, Jan.-Feb. 1991. For entry velocities from $6 - 9$ km/s, a similar correlation is given for stagnation-point heating rates to a hemisphere.

If radiation can be neglected, another relation is given in Tauber, Bowles, and Yang, *Use of Atmospheric Braking During Mars Missions*, J. Spacecraft and Rockets, v. 27, no. 5, pp. 514-521, Sept.-Oct. 1990. Eqn. (6) in that reference can be used to obtain an equation similar to equation (46):

$$\dot{q} = 1.35 \times 10^{-8} \left[\frac{\rho}{r_n} \right]^{0.5} V^{3.04} (1 - \frac{c_{pw} T_w}{0.5 V^2}). \tag{47}$$

See also p. 3 of AIAA Paper 99-0348, *New TPS Strategies for Planetary Entry Vehicle Design*, by Olynick, Loomis, Chen, Venkatapathy, and Allen, where this equation is discussed in a more general context.

7.4.3 Stagnation-Point Temperature, Reusable TPS

The temperature of the vehicle at the stagnation point depends on heat capacity and the balance of heat conduction and radiation. In AAE450, for reusable TPS designs, we've evaluated the temperature of the surface at the stagnation point using a crude lumped heat-capacity model. This crude model is more refined than the even simpler approximation of radiative equilibrium; to our knowledge, it is the simplest approximation that allows determining a TPS weight. From the first law,

$$\Delta E = \sum \dot{q} \Delta t, \tag{48}$$

where E is the internal energy of an element of the surface at the stagnation point. Per unit of surface area,

$$\Delta E = c_p \Delta T \rho_w t_w, \tag{49}$$

where c_p is the specific heat of the surface material per unit mass, ΔT is the temperature change, ρ_w is the density of the surface material, and t_w is the thickness of the surface material. This crude approximation assumes constant specific heats and neglects all heat transfer within the body, but it is the kind of approximation used in preliminary design.

The heat transfer is composed of conduction from the fluid (convective heat transfer) and radiation,

$$c_p \frac{dT}{dt} \rho_w t_w = \dot{q} + \dot{q}_r - \epsilon \sigma T_w^4, \tag{50}$$

where $\dot{q}_r$ is the radiation from the fluid to the surface. We will neglect $\dot{q}_r$ for reentry from LEO; it becomes significant mainly for reentry from escape velocity or perhaps high orbit. The last term in equation (50) represents cooling of the surface via radiation from the surface (see for example Reynolds, *Engineering Thermodynamics*, 1977, sec. 14.8). Here, ϵ is the emissivity of the surface, σ is the Stefan-Boltzman constant, $\sigma = 5.669 \times 10^{-12}$, W/(cm²K⁴), and T_w is the wall temperature, in Kelvin. Using these units, the radiation heat transfer will again be in units of W/cm². If c_p is taken in J/(kgK), ρ_w in kg/cm³, t_w in cm, and t in sec., the units will be properly consistent.

Equations (46) and (50) are combined and solved at each time step in the reentry in order to obtain the stagnation-point temperature, for a reusable TPS.

7.4.4   Lumped Heating at Solid Nosetip

For a small-bluntness nosetip that serves as a massive heatsink, formulas (49) and (50) don't accurately reflect the geometry. Consider a nosetip which is basically a blunted cone, for example, with a nose radius that is some small fraction of the base radius. The entire nosetip is solid TPS, yet the formula treats the nosetip as a plate whose thickness is small compared to surface distances over which the heat transfer varies significantly.

For such a solid nosetip, it seems better to consider the whole nosetip as one solid heat sink, by integrating (49) and (50) over the solid nose. We assume that the internal heat conduction is large, so that the nosetip is approximately at a single temperature. In this case we have

$$c_p \frac{dT}{dt} \rho_w V = \int \left(\dot{q} + \dot{q}_r - \epsilon \sigma T_w^4 \right) dA, \tag{51}$$

where V is the volume of the solid nosetip and dA is an element of the surface area. The left-hand side of equation (51) is easily evaluated, but the right-hand side requires further simplification. Depending on geometry, it is probably best to evaluate the integrand on the right-hand side at roughly 2-4 points on the nosetip, and use some approximation to the actual integral. Discuss this analysis with your instructor, and document it in your report.

For blocks with sharp noses this solid nosetip exhibits some interesting phenomena. The heat transfer to the stagnation point is commonly roughly 10 times that observed at 90-deg. to the stagnation point. This rough analytical result is confirmed by experiment – compare the cylinder heat-transfer measurements shown in Fig. 6.18 of Anderson's text (1989). So overall heat transfer to the block is not that high with a sharp nose. Furthermore, at some temperature a steady-state condition is reached where radiative cooling from the rear sides of the block balances the heat transfer at the stagnation point. Paul Kolodziej from NASA Ames has commented that *'Bingo! This [last] phenomena contributes to the remarkable performance of the UHTC leading edges. We've done extensive finite element analysis (both thermal and structural) to improve our understanding of this coupled interaction between the flow field and the UHTC sharp leading edge.'* Thus, it appears that this critical effect has in general been confirmed by detailed simulations and flight tests. For example, see NASA TM 110407, *A thermostructural analysis of a diboride composite leading edge*, by Kowalski et al., July 1996.

For these solid nosetips one often finds that a decrease in nosetip radius decreases overall heating. The minimum feasible nosetip radius is then a matter of interest. In response to a query regarding this minimum radius, Paul Kolodziej of NASA Ames stated that *'We've been focusing on leading edges with a radius of 1 mm. If you operate the sharp leading edge on its aerothermal performance constraint it will rapidly reach a steady state constant temperature'* [email, 04/27/00]. Thus, this is the minimum radius which one should probably look at.

7.4.5   Temperatures of Ablating TPS

For an ablating TPS, there is no equivalent to the above simple lumped-capacity method. The simplest practical approach is to use a one-dimensional heat-conduction code that includes surface ablation effects. One such method is the `SODDIT` code (see, for example, *A User's Manual for the Sandia One-Dimensional Direct and Inverse Thermal Code*, by B. F. Blackwell, R.W. Douglass, and H. Wolf, Sandia Report SAND85-2478, May 1987). A iterative process is used; the heating

rate history is first computed for the TPS, after which the TPS ablation history is then computed separately. This is the same method used by Sandia personnel for various NASA Ames designs, and sample input files were provided by Sandia personnel for the Mars entry problem.

7.5 Windward-Surface Heating Analysis

The following contains the critical elements of the windward-surface heating analysis for hypersonic flow, as adapted from Prof. Gustafson's notes. These methods are for the earth's atmosphere, unless otherwise noted.

7.5.1 Flat-Plate Heat-Transfer Rate for Large Angles of Attack

This is also taken from Tauber, Menees and Adelman, *Aerodynamics of Transatmospheric Vehicles*, J. Aircraft, v. 24, n. 9, Sept. 1987, pp. 594-602. The formulas are also available in Anderson, Hypersonic and High Temperature Gasdynamics, McGraw-Hill, 1989, p. 291. Equation (4) in Tauber et al. gives the heating rate per unit area as

$$\dot{q} = C\rho^N V^M. \tag{52}$$

Here, $\dot{q}$ is the heat-transfer rate into the body, per unit area, ρ is the freestream density, and V is the flight velocity. The appendix of Tauber et al. gives the constants, for a fully catalytic surface (a conservative approximation). The constants give the heating rate in W/cm^2 if the velocity is given in m/s and the density in kg/m^3.

For a laminar flat plate, the constants are $M = 3.2, N = 0.5$, and

$$C_1 = (2.53 \times 10^{-9})(\cos\phi)^{1/2}(\sin\phi)(x^{-1/2})(1 - g_w), \tag{53}$$

where ϕ is the local body angle with respect to the freestream, x is the distance (from the stagnation point) measured along the body surface, and g_w is the ratio of wall enthalpy (h_w) to total enthalpy (h_0). The body angle ϕ is the angle between the tangent and the velocity vector – for a flat plate, it is the angle of attack. For zero angle of attack, as for a flat plate, this formula goes to zero, which is incorrect. A query to Micheal Tauber at Ames produced the following response *'The angle phi is the local body angle with respect to the free-stream, i.e. for a flat plate, it's the angle of attack. The expression was derived assuming that Newtonian theory was valid for the product of pu (the surface pressure x boundary layer edge velocity) that appears in the laminar and turbulent convective heat transfer equations. The Newtonian approximation is only valid when the free-stream Mach number component that is normal to the surface is supersonic. Therefore, the simple expressions given in the 1987 paper fail at zero, or small angles, of attack. The limit is $M_\infty \sin\phi > 1$.'* For smaller angles of attack, it seems better to estimate using the flat plate formulas given in White, *Viscous Fluid Flow*, 2nd edition, Sec. 7-3.3 and 7-8.1; see section 7.5.2.

From thermodynamics, $h_w = c_{pw}T_w$. The total enthalpy is $h_0 = h_a + 0.5V^2$, where h_a is the local enthalpy of the atmosphere. However, for reentry h_a is usually much smaller than $0.5V^2$, and will be neglected. Thus, as before,

$$g_w \simeq \frac{c_{pw}T_w}{0.5V^2}. \tag{54}$$

For a turbulent flat plate, the constant $N = 0.8$, and there are two different cases for the others.

For $V \leq 3962$ m/s, $M = 3.37$, and

$$C_2 = (3.35 \times 10^{-8})(\cos \phi)^{1.78}(\sin \phi)^{1.6}x^{-1/5}(T_w/556)^{-1/4}(1 - 1.11g_w). \tag{55}$$

For $V > 3962$ m/s, $M = 3.7$, and

$$C_2 = (2.20 \times 10^{-9})(\cos \phi)^{2.08}(\sin \phi)^{1.6}x^{-1/5}(1 - 1.11g_w). \tag{56}$$

Laminar-turbulent transition will be discussed later.

7.5.2 Flat-Plate Heat-Transfer Rate for Small Angles of Attack

Here we need a method of computing the approximate heat transfer to the windward surface when $M_\infty \sin \phi \leq 1$. The flat plate at zero angle of attack will be used to provide a crude approximation, primarily based on White, *Viscous Fluid Flow*, 2nd edition, McGraw-Hill, 1991.

For a laminar case, follow section 7-3.3. The reference temperature, T^*, is computed using 7-42,

$$\frac{T^*}{T_e} \simeq 0.5 + 0.039M_e^2 + 0.5\frac{T_w}{T_e}. \tag{57}$$

Here, T_e is the temperature at the edge of the boundary layer, T_w is the wall temperature, and M_e is the Mach number at the edge of the boundary layer. The Chapman-Rubesin parameter, C, is then evaluated at the reference temperature using (7-40),

$$C^* \simeq \left(\frac{T^*}{T_e}\right)^{(-1/3)}. \tag{58}$$

Here, we will apply these formulas by crudely taking edge conditions as equal to freestream conditions, which is not so bad for small angle of attack. Then compute the adiabatic wall temperature using (7-41a),

$$\frac{T_{aw}}{T_e} = 1 + \sqrt{Pr^*}\left(\frac{\gamma - 1}{2}\right)M_e^2, \tag{59}$$

where we will take Pr as a constant equal to about 0.72. Then the skin-friction coefficient can be computed as (7-41b),

$$C_{fe} = \frac{0.664\sqrt{C^*}}{\sqrt{Re_{xe}}}. \tag{60}$$

Here, Re_{xe} is the Reynolds number based on edge conditions and the arc length from the leading edge. Use freestream conditions as a crude approximation for edge conditions. We won't use this skin-friction coefficient for the drag, but will use the Reynolds analogy to get the heat-transfer coefficient (7-41c),

$$C_{he} = 0.5C_{fe}/(Pr^*)^{2/3}. \tag{61}$$

This Stanton number is then used to compute the wall heat flux, using (7-44),

$$q_w = C_{he}\rho_e U_e C_{pe}(T_{aw} - T_w). \tag{62}$$

For the heat capacity of air, C_{pe}, a value of about 1100 J/kg-K seems reasonable, based on Bolz and Tuve, *Handbook of Tables for Applied Engineering Science*, Table 1-2.

For a turbulent case, the formulas in White section 7-8.1 are rather complex, requiring solution of a transcendental equation. These seem to be rather more sophisticated than is warranted for 450. Continued use of the reference temperature concept seems warranted instead (compare the present section 7.8.1). The incompressible formulas are used, but with the properties evaluated at the reference temperature. See Bertin, *Hypersonic Aerothermodynamics*, AIAA, 1994, section 7.4.1. We then have that

$$C_{fe} \simeq 0.027/Re_{xe}^{1/7}, \tag{63}$$

following White eqn. 6-70. The Stanton number C_{he} is again computed using the Reynolds analogy, eqn (61), as in White 7-122. The heat-transfer rate is then computed, again using equation (62), but now using

$$\frac{T_{aw}}{T_e} = 1 + \left((Pr^*)^{1/3}\right) \frac{\gamma - 1}{2} M_e^2, \tag{64}$$

with the change in the power of the Pr based on Bertin, p. 340, and $\gamma \simeq 1.4$. This is crude, with uncertain accuracy, but it is better than using the Tauber formula at zero angle of attack, where the flat plate heat-transfer rate is taken as zero!

7.5.3 Heat-Transfer to Wing Leading Edges

This is taken from equation (6) in Tauber, which is

$$\dot{q_{LE}} = \left[0.5(\dot{q}_0)^2 \cos^2 \Delta + (\dot{q}_{FP})^2 \sin^2 \Delta\right]^{1/2}, \tag{65}$$

where Δ is the sweep angle of the wing leading edge, $\dot{q}_0$ comes from using the stagnation-point heat-transfer formula for the local conditions, and $\dot{q}_{FP}$ comes from using the flat-plate heat-transfer formula for the local conditions.

Presumably all lengths are to be given in meters. These correlations are validated against Shuttle data in the paper.

The leading-edge thickness of any wings is clearly a critical issue. For 450, this heat-transfer analysis can only be done for representative points in your design. Pick a few points along the leading edges, and a few points on the body surfaces, and compute the heating results only there. This limited analysis can then be used to determine a TPS distribution and weight that is accurate enough for preliminary design. Clearly, the windward surface will be the critical region.

7.5.4 Heating Rates for Mars Entry

Most recent papers analyzing the heating rates for Mars entry use CFD methods for design purposes. Some simple correlations are, however, given in Tauber, Bowles, and Yang, *Use of Atmospheric Braking During Mars Missions*, J. Spacecraft and Rockets, v. 27, no. 5, pp. 514-521, Sept.-Oct. 1990. Away from the stagnation point, Tauber et al. use correlations developed for flat plates and swept leading edges in air. These correlations for air are similar to those shown above.

7.6   Leeward Surface Heating

Any surfaces that are shadowed from the flow have much lower heat transfer, which is difficult to analyze. Designs should use thermal blankets in this region. One simple method is to use blankets similar to those used on the lee side of the Shuttle. The weight of the lee TPS should be a small fraction of the windward TPS.

7.7   Material Properties for Thermal Protection System

Most of these may be obtained from the public-domain NASA Ames website `http://tpsx.arc.nasa.gov.` Most of the properties of the Ultra-High Temperature Ceramics can be found from public-domain papers to be distributed by the instructor (e.g., reports by Clougherty et al.). A detailed discussion of the various materials was recently given by Rasky et al., *Thermal Protection System Materials and Costs for Future Reusable Launch Vehicles*, J. Spacecraft and Rockets, v. 38, no. 2, pp. 294-296, 2001. Other data will be handed out in class.

A TPSX database is also available at the cited website; however, distribution is limited. **If you do use data obtained from TPSX, be careful not to release this data contrary to regulations. In particular, be careful what you put in your reports, which must be available for public distribution.**

The thermal properties of the materials are temperature dependent. If the temperature dependence is significant (greater than 10-20%, say), then this temperature dependence should be included in your analysis.

Clougherty et al. give the properties of the UHTC compounds in *Research and development of refractory oxidation-resistant diborides, Part II, Volume V, Thermal, Physical, Electrical, and Optical Properties*, AFML-TR-68-190, 1969, DTIC citation AD-865321. This is the most recent publicly available source, so it will be taken as the best-available data for the hafnium and zirconium diborides. A variety of different material types were tested, as listed in Table 1 in Clougherty et al. For zirconium diboride, Table 10 lists values of specific heat ranging from 0.17 to 0.21 cal/gm-C, depending on temperature (1000 to 2000$°C$) and composition. A value of 0.19 cal/gm-C is therefore recommended as sufficiently accurate for the present preliminary design. In MKS units, this is $C_p \simeq 795$ J/kg-K. Table 13 shows density data which ranges from 4.44 to 10.95 gm/cc, depending on material composition. This is the largest source of uncertainty in the specification of these compounds. Unfortunately, accurate specifications for current compounds are not publicly available. Kolodziej does indicate that SiC is used with the diboride (several papers). For ZrB_2, this suggests that compound V in Clougherty et al. is a reasonable approximation, suggesting a density of about 6 gm/cc (Table 13), or 6000 kg/m^3.

For emissivity, Kolodziej reports a representative value of 0.8 in NASA TM 112204, *Aerothermal performance constraints for hypervelocity small radius unswept leading edges and nosetips*, July 1997, p. 5. He indicates that a 1 mm nose radius is reasonable for an unswept hemicylinder leading edge, and gives a single-use temperature limit of 2760$°C$. While Clougherty gives emissivity ranging from 0.6 to 0.4 for ZrB_2 in Fig. 45, depending on temperature, the more recent value of 0.8 from Kolodziej is suggested.

7.8 Hypersonic Skin-Friction Analysis

The following contains the critical elements of the simplified skin-friction analysis, as adapted from Prof. Gustafson's notes. The method is primarily taken from AIAA Paper 90-0538, *Hypersonic waveriders for planetary atmospheres*, by John Anderson et al. For some additional detail, see Gustafson's notes as saved in the file `skinfric-backup.pdf` in the course directory. This method should be used above Mach 5; for supersonic skin friction see Sec. 7.9.2.

7.8.1 Correlations for Local Compressible Skin Friction

This section is nearly a direct quote from the Anderson paper.

The skin friction distribution along the streamlines is calculated using the reference temperature method of Eckert. In the reference temperature method, approximate formulas are used to predict the skin friction, with the physical properties evaluated at an appropriate reference temperature. For a flat plate in laminar flow, the local skin friction coefficient is given by

$$C_f = 0.664(Re_x)^{-1/2}(T'/T_\infty)^{(\omega-1)/2}. \tag{66}$$

Re_x is the local Reynolds number defined as

$$Re_x = \frac{\rho_\infty V_\infty x}{\mu_\infty}, \tag{67}$$

where ρ_∞ is the freestream density, V_∞ is the freestream velocity, x is the local distance from the leading edge of the plate, and μ_∞ is the freestream value of the viscosity.

Also, T' is the reference temperature, defined as

$$\frac{T'}{T_\infty} = 1 + 0.032M_\infty^2 + 0.58\left(\frac{T_w}{T_\infty} - 1\right) \tag{68}$$

where M_∞ is the freestream Mach number and T_w is the wall temperature. In 450, put in some average wall temperature from your trajectory differential equation solution, even though this results in some ad-hoc averaging over the surface. Finally, ω is the exponent of an assumed exponential variation of μ, namely,

$$\frac{\mu'}{\mu_\infty} = \left(\frac{T'}{T_\infty}\right)^\omega. \tag{69}$$

A value of $\omega = 0.75$ is used in the present study.

The flat plate skin friction coefficient for turbulent flow is given by

$$C_f = \frac{0.0592}{(Re'_x)^{0.2}}, \tag{70}$$

where

$$Re'_x = \frac{\rho' V_\infty x}{\mu'}. \tag{71}$$

Here, ρ' and μ' are evaluated at the reference temperature T'. Note that this change to the reference temperature is done at constant pressure. Thus, $p' = \rho' R T'$, $p_\infty = \rho_\infty R T_\infty$, and $p' = p_\infty$, so $\rho'/\rho_\infty = T_\infty/T'$.

This type of skin friction analysis is much simpler, in concept and use, than integral boundary layer methods. Results obtained using the reference temperature method were within 10% of results obtained using a more complex integral boundary layer method (Ref. cited in paper) even at high hypersonic Mach numbers. Also, the computation time required by the reference temperature method is very small when compared to an integral boundary layer method.

Boundary layer transition is predicted using a correlation of the local transition Reynolds number, $Re_{x,t}$, with the local edge Mach number, M_e, as follows:

$$\log_{10}(Re_{x,t}) = 6.421 \exp(1.209 \times 10^{-4} M_e^{2.641}). \tag{72}$$

This correlation is based on the experimental data of DiCristina (ref. cited in paper) for transition on sharp cones at zero angle of attack. This correlation is used due to the lack of better methods of transition prediction in hypersonic flows. It is also presented in Anderson, HHTG, p. 280, eq. 6.140. For 450, we will go ahead and use this even at angle of attack. Gustafson suggests estimating M_e for your angle of attack using $M_e = M_\infty \cos \alpha$. This crude formula neglects the bow shock, but it will have to do. Note that for M_e larger than about 35, $Re_{x,t}$ is greater than about 10^{30}. For this case, the flow will certainly be laminar, so computation of this very large number is not needed.

7.8.2 Low-Speed Skin Friction Coefficient and Drag

The following information for low-speed computations is given **for background only**, to help you in understanding and applying the high-speed methods.

At low speed, the local flat-plate laminar skin friction coefficient is

$$C_f(x) = \frac{\tau}{0.5\rho_\infty V_\infty^2} = 0.664(Re_x)^{-1/2}. \tag{73}$$

Here, τ is the local shear stress. The drag on one surface of the flat plate is

$$D = b \int_0^l \tau(x)dx = 0.332 b\rho_\infty V_\infty^2 \int_0^l (Re_x)^{-1/2}dx, \tag{74}$$

where b is the width of the flat plate, and l is the length. We can make a drag coefficient for a length l of this plate, using bl for the reference area, as follows:

$$C_{D,l} = \frac{D}{0.5\rho_\infty V_\infty^2 bl} = \frac{0.664}{l} \int_0^l (Re_x)^{-1/2}dx. \tag{75}$$

Simplifying,

$$C_{D,l} = \frac{0.664}{l} \sqrt{\frac{\mu_\infty}{\rho_\infty V_\infty}} \int_0^l x^{-1/2}dx. \tag{76}$$

Note that

$$\int_0^l x^{-1/2}dx = 2l^{1/2}, \tag{77}$$

so

$$C_{D,l} = \frac{0.664}{l} \left[\sqrt{\frac{\mu_\infty}{\rho_\infty V_\infty}}\right] 2l^{-1/2}, \tag{78}$$

or

$$C_{D,l} = 1.328(Re_l)^{-1/2}. \tag{79}$$

Equation (79) is the drag coefficient for laminar flow on one side of a low-speed flat plate of length l and span b. Compare White, *Viscous Fluid Flow,* 2nd ed., 1991, eqn. 4-53.

Let the angle of attack (AOA) be α. Assume that at AOA,

$$C_{D,l} = (\cos\alpha)C_{D,l,flatplate}. \tag{80}$$

This appears to be no more than a guess.

7.8.3   High-Speed Laminar Skin-Friction Drag Coefficient

Similarly, for laminar flow on a flat plate at high speed, the local skin friction on one surface is

$$C_{D,l} = \cos\alpha(1.328)\left(\frac{T'}{T_\infty}\right)^{-0.125}(Re_l)^{-1/2}. \tag{81}$$

The reference area is again bl. T' is again the reference temperature; Prof. Gustafson suggests putting in some average temperature from your TPS temperature solution, even though this will be a crude average over the surface. Here, Re_l has no prime, but is the freestream value; computation of the flow behind the bow shock is too complex for this course.

7.8.4   High-Speed Turbulent Skin-Friction Drag Coefficient

Equation (70) gives the local skin friction coefficient. Recall that ρ' and μ' are evaluated at the reference temperature T'. The viscosity is found using equation (69). Assuming constant pressure across the boundary layer (and across the oblique shock, which is a poor approx.), the perfect gas law then gives $\rho'T' = \rho_\infty T_\infty$. Using a derivation similar to that used for the laminar case, we will arrive at an equation analgous to equation (76),

$$C_{D,T,l} = \frac{0.0592}{l}\int_0^l (Re'_x)^{-0.2}dx. \tag{82}$$

Simplifying, and skipping a number of steps, and noting that $1.25(0.0592) = 0.074$,

$$C_{D,T,l} = 0.074(Re'_x)^{-0.2}. \tag{83}$$

For a plate at AOA α,

$$C_{D,T,l} = 0.074\cos\alpha(Re'_x)^{-0.2}. \tag{84}$$

7.8.5   Summing Laminar and Turbulent Skin Friction

For a complete plate, one starts by computing the transition Reynolds number, and the transition length x_t. If $x_t > l$, the length of the plate, then the entire plate is laminar, and the laminar formulas should be used.

If $x_t < l$, then we have some laminar flow followed by some turbulent flow. For 450, assume that the plate is fully laminar up to x_t, and use the laminar skin friction to here, making sure to

correct the area normalization in C_D to the reference area. Add in the skin friction due to the turbulent boundary layer, which is assumed to have an origin at the leading edge, but which is only switched on at x_t. This is done by computing the turbulent boundary-layer skin-friction from the leading edge, and then subtracting the turbulent boundary-layer skin friction from the leading edge to x_t.

The total skin-friction drag coefficient is thus

$$C_D = C_{D,turb.,l} + [C_{D,lam.,x_t} - C_{D,turb.,x_t}] \frac{A_{x_t}}{A_{ref}}, \tag{85}$$

where $A_{ref} = bl$ and $A_{x_t} = bx_t$. Adding in the AOA correction and simplifying,

$$C_D = \left[0.074(Re'_l)^{-0.2} - 0.074(Re'_{x,t})^{-0.2} \left(\frac{x_t}{l}\right) + 1.328 \left(\frac{T'}{T_\infty}\right)^{-0.125} (Re_{x,t})^{-0.5} \left(\frac{x_t}{l}\right) \right] \cos\alpha. \tag{86}$$

Here, $Re_{x,t} = (\rho_\infty V_\infty x_t)/\mu_\infty$, $Re'_{x,t} = (\rho' V_\infty x_t)/\mu'$, and $Re'_l = (\rho' V_\infty l)/\mu'$. As when computing the local heating, interpret x as the distance from the stagnation point, when applying these flat-plate formulas to your more complex geometries.

Be careful with the reference areas in the drag coefficient formulas! The most convenient one is the entire surface area. But in the end, you will have to normalize the complete drag coefficient for the entire vehicle by one reference area, which must be used consistently in all codes.

To analyze a wing-like shape, use strip theory. Think of longitudinal strips along streamlines. Divide the wing into several strips. For a delta wing, you might have transition near the root and not near the tip. Put a few strips on the wing and get an approximate result. Neglect the shadowed regions of your vehicle, since $\rho \simeq 0$ here. Get ρ, M, etc. from the main program. Note that

$$C_{D,total} = C_{D,newtonian} + C_{D,skinfriction}, \tag{87}$$

in the hypersonic case. For a cone or cylinder, just try to unroll the cone or cylinder and apply the formulas as best you can.

7.9 Analysis of Supersonic Aerodynamics

7.9.1 Introduction

According to Prof. Gustafson, the supersonic portion of the mission is still important enough that it cannot be neglected. The Newtonian result will not give enough lift coefficient at lower altitudes and speeds to give a reasonable first approximation. In real supersonic flow, L/D will increase and occur at lower angles of attack.

In the aerodynamics subroutine, Gus suggests making the change between analysis methods for a range between Mach 5 and 4. In between, use a weighted average relative to Mach number. The change must be carried out smoothly, and the angle of attack must be reduced smoothly, so oscillations do not develop in the trajectory and solution. Remember that the trajectory person selects angle of attack.

7.9.2   Skin Friction Drag

Prof. Gustafson stated that the following were taken from A. Shapiro, *The Dynamics and Thermodynamics of Compressible Fluid Flow*, but the exact reference remains to be found. They do not use the reference temperature. Both sides of the vehicle are analyzed now, we do not neglect the shadowed side at supersonic speeds. The entire vehicle is assumed to have a turbulent boundary layer.

The incompressible skin friction is

$$C_{F,i} = 0.074(Re_x)^{-0.2}, \tag{88}$$

as discussed in section 7.8. Correct this for compressibility, using

$$C_F = \frac{C_{F,i}}{[1 + 0.144M_\infty^2]^{0.65}}. \tag{89}$$

Correct for conical geometries using

$$C_{F,cone} = \frac{2}{\sqrt{3}}C_{F,flatplate}. \tag{90}$$

Add up the various elements of the vehicle as follows:

$$C_{D,F} = C_{F,fuselage}\frac{S_{fuselage}}{S_{ref}} + C_{F,nose}\frac{S_{nose}}{S_{ref}} + C_{F,wing}\frac{S_{wing}}{S_{ref}} + C_{F,tail}\frac{S_{tail}}{S_{ref}}. \tag{91}$$

7.9.3   Wave Drag due to Thickness

The wave drag is modeled with crude approximations from *Fundamentals of Aircraft Design*, by Leland Nicolai, University of Dayton, 1975, self-published. See the figures from this book, which will be handed out. See also `ss-subsaero.pdf` in the class-account directory.

On a conical forebody, $C_{D_{N_2}}$ from Fig. 11.18 is the nose wave drag coefficient, based on the body cross-sectional area $\pi d^2/4$, where d is the base diameter of the cone. Note that $\beta = \sqrt{M_\infty^2 - 1}$, and $f_N = l_N/d$, where l_N is the axial length of the cone. For example, $\sin\theta = d/(2l_N)$, where θ is the half-angle of the cone.

The wing wave drag is approximated differently depending on whether the leading edge is supersonic. For a supersonic leading edge,

$$\sqrt{M_\infty^2 - 1}\cot\Lambda \geq 1, \tag{92}$$

where Λ is the sweep angle (0 degrees for an unswept wing). In this case,

$$C_{D,W} = \frac{16\tau^2}{3\sqrt{M_\infty^2 - 1}}\frac{S_e}{S_{ref}}, \tag{93}$$

where τ is the thickness ratio of the wing, and S_e is the wetted or exposed area. For the case where the leading edge is subsonic, use

$$C_{D,W} = \frac{16}{3}\tau^2\cot\Lambda\frac{S_e}{S_{ref}}. \tag{94}$$

To get the lift, take $dC_L/d\alpha$ from Figure E.4 , assume it's constant, and use $C_L = (dC_L/d\alpha)\,\alpha$. Note that the symbols in this figure are the same as in Fig. E.5, and that A seems to be the aspect ratio, in both figures. You may want to fit a curve to the data in the figure, although this is a little tedious. Assume that your vehicle remains below the stall angle. To get the drag due to lift (induced drag, $C_{D,i}$), take $C_{D,i}/C_L^2$ from Figure E.5.

7.9.4 Other Notes

We will ignore subsonic and transonic flow in 450. For supersonic flow, equation 2.15 in Nicolai's design book gives the moment coefficient, but no way to determine the angle of attack at which it becomes zero. For subsonic and supersonic conditions, we will just have to assume that the vehicle can be trimmed. Although subsonic and transonic aerodynamics is often a critical design issue for reusable launch vehicles that are required to land, it is just too difficult to try to cover this topic in 450.

7.10 Viscous Interaction Effects

At high altitudes, the density becomes very low, so although the speed is often very high, the Reynolds number is low. This causes the boundary layers to become very thick. The thick boundary layers now act to displace the shock in significant ways. See Anderson, *Hypersonic and High Temperature Gas Dynamics*, Chapter 7 for a discussion of these effects. At sufficiently high altitude, the gas density becomes so low that the mean distance between molecular collisions, the mean free path, becomes significant or large compared to the vehicle dimensions. This is the rarefied flow regime.

7.10.1 Lockheed Viscous-Interaction Correlation

In the past, AAE450 analysis has used a crude correlation provided by Lockheed Missiles and Space in order to correct the Newtonian inviscid L/D for these low-density viscous effects. Figure 13 shows the correlation provided by them to AAE450 in 1990. The chart included the formula plotted:

$$y = 1.0 - 30.851(VI) + 577.02(VI)^2 - 4285.94(VI)^3. \tag{95}$$

where $y = (L/D)/(L/D)_{inv}$. If the formula gives $y < 0.275$, then y is to be set to $y = 0.275$. Here, $(L/D)_{inv}$ is the Newtonian value.

To use this Lockheed viscous interaction correlation, compute $VI = M_\infty/\sqrt{(Re_\infty)}$ and use the correlation to correct L/D. Use this to correct the drag coefficient only:

$$C_{D,actual} = C_{D,Newtonian}\frac{(L/D)_{Newtonian}}{(L/D)_{actual}} \tag{96}$$

The drag coefficients at high altitude will be high, but the forces will be small anyway. At 75 km this will start to affect C_D noticeably. Will have an effect for awhile and then go away at low altitude. Assume C_L is totally unaffected in this approximation. Do this for the Newtonian part of C_D only (the inviscid part only). After doing the correction, add in the skin-friction drag.
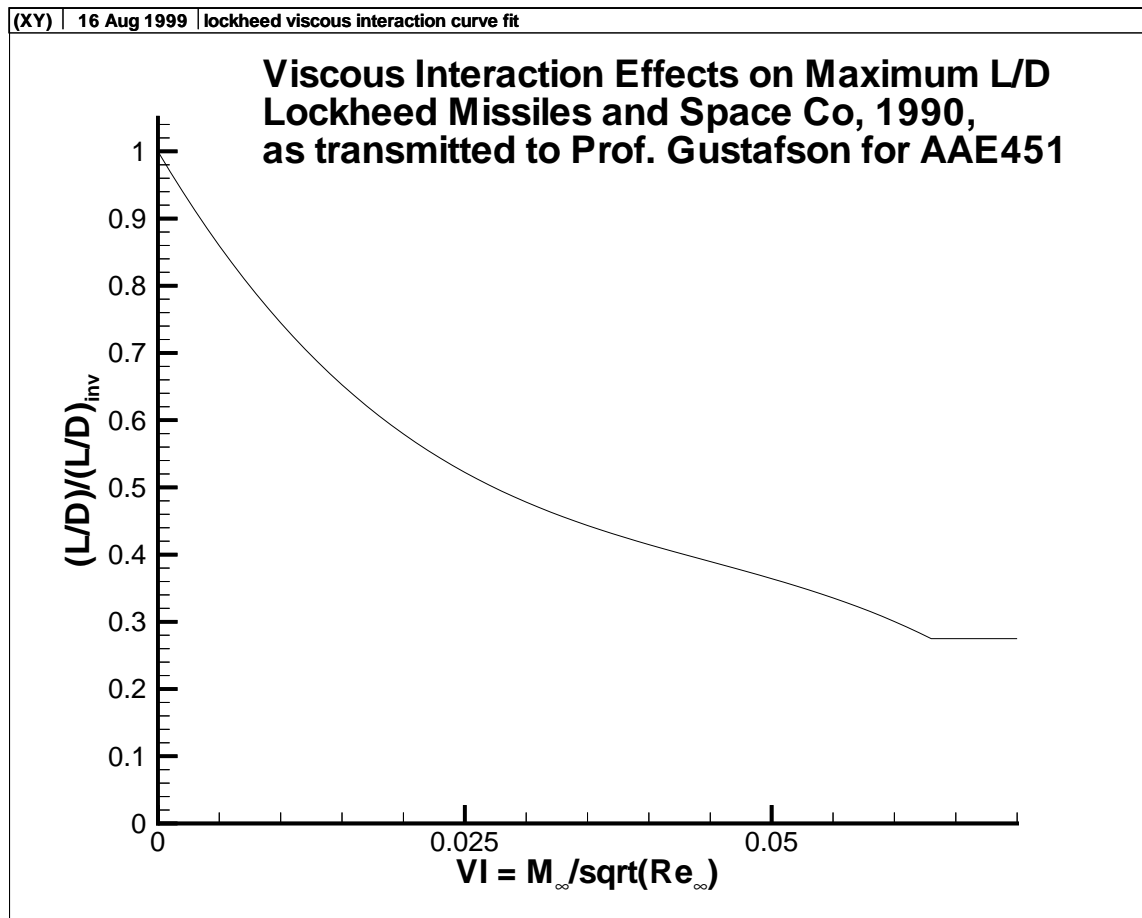
Figure 13: Lockheed Correlation for Viscous Interaction

Unfortunately, the source of this correlation is unknown. Therefore, the accuracy and reliability are also unknown, and suspect. However, the correlation is very simple to use.

Another relatively simple correlation is given by Maslen in *Synergetic Turns with Variable Aerodynamics*, J. Spacecraft, vol. 4, pp. 1475-1482, Nov. 1967, on p. 1480 (e.g., eqn. B4). This should be investigated if improved estimates are needed.

7.10.2   Viscous Interaction Effects: Bridging Formulas

A good review of the experimental data for this effect is contained in Boylan and Potter, *Aerodynamics of typical lifting bodies under conditions simulating very high altitudes*, AIAA J. v. 5, n. 2, pp. 226-232, Feb. 1967. Boylan and Potter also suggest a more accurate and reliable method of computing the viscous interaction. The lift and drag should be computed using free molecular methods, and then a bridging formula should be used to bridge from the very low density free-molecular region to the continuuum results. This concept is discussed in various papers, as are methods for computing free molecular effects. If this issue is important to the present design, these papers may be handed out and discussed in class.

7.11   Sample Case: Blunt Flat Plate with Body Flap

The full set of aerothermodynamic methods was coded up by the instructor for a simple sample case. The objective of this is twofold: (1) to provide a good framework of `FORTRAN` programs with a reasonable architecture, from which students can develop their own programs, and (2) to show by example how to use the methods for a particular design. The sample case was purposely selected to be an oversimplified geometry, so that all groups will have to develop their own codes for their own vehicles. It is nevertheless representative of an idealized hypersonic vehicle with best-case performance, so it can be used by the trajectory analysts in their early design stages, before a complete vehicle design has been generated by their group.

The sample case is shown in Fig. 14. It is a blunt flap plate with a body flap. The nose is a hemicylinder, with radius `rnose`, shown as R. Since the top part of the hemicylinder is shadowed when at angle of attack, the force coefficients for the hemicylinder are different from those for the full cylinder. The coefficients that were coded into the `aerodat.f` subroutine were taken from Clark and Trimmer, section 2.1.3, equations (38) and (42), as discussed in the comments in the code. The equations given by Clark and Trimmer are for a *pair* of swept cylinders, so the results must be divided by a factor 2. See the check-derivation given in the file `hemicylinder.pdf` in the class directory. The flap length is `lflap`, the plate length is `lplate`, the angle of attack is defined with respect to the plate as α,, and the body flap deflection with respect to the plate is defined as β, positive downwards. The width of the vehicle is `width`.

8   Propulsion

The propulsion system is to be designed using an existing flight-proven engine, with a known weight, ISP, thrust, and so on. Your instructor is open to hearing of methods by which new propulsion systems can be reliably designed within the constraints of this course. Prof. Gustafson
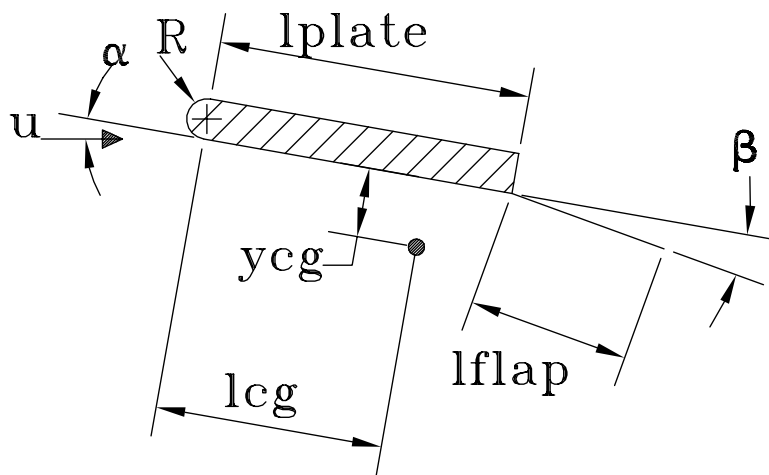
Figure 14: Schematic of Blunt Flat Plate with Body Flap

was not able to find a set of analysis tools which could result in reasonable designs with realistic performance.

The properties of existing propulsion systems can be found in many places. The best current source is Isakowitz (1999). Other sources include the Jane's handbooks (Jane's Space Directory is one that we have), and Marc Wade's Encyclopedia Astronautica on the web. Data is also provided on p. 234 and pp. 302-304 of Humble, and on p. 282 and p. 286 of Sutton. Prof. Heister has noted that non-cryogenic liquid rockets are OK for launch-on-warning missions (as in the early ICBM's), although solid rockets require less maintenance for these missions.

8.1   Boost Propulsion

An existing booster is normally to be selected. Data for the thrust, ISP, weight, empty weight, nozzle diameter, and so on need to be found in the literature. The boost trajectory is then analyzed using the same equations of motion used for the reentry analysis. An existing code can be modified for this purpose. However, as usual when using an existing code, be sure to check the code! Be warned that the BOOST codes derived from that written by Dan Harris in Fall 1998 have some major bugs. The best existing code is probably that written by T. J. Hoverman for Columbiad in Fall 1999. Wind loads should be taken into account. A control algorithm for the gimballing of the rocket nozzle is also to be designed and used. The vacuum thrust of the engines is to be corrected for altitude.

8.2   Vehicle Propulsion

Here also, an existing flight-proven engine is normally required. The propellant tanks and the propellant feed system should be designed following Chapter 5 of Humble et al. (1995). Another authoritative source may be substituted upon consultation with the instructor. Try to balance the tank positions about the center of gravity so that the c.g. doesn't move as the fuel is used.

8.3   Reaction Control System

An RCS system is needed to control the attitude of the vehicle while it is out of the atmosphere, or in the thin upper atmosphere. The RCS system provides pitch, roll, and yaw. In 450 we do a simplified design, and select from available flight-proven thrusters. Data is available for various thrusters including the RS-45,-43,-25,-42, and Peacekeeper engines. Pairs of opposite thrusters should be placed in the fore and aft ends of the vehicle, to give the biggest torque for a given thrust. Save space for the engines and propellant. Usually helium-driven pressure-fed thrusters have been used. A feed pressure of 50 psi is sufficient.

The thrust of the RCS system is set by the need to be able to turn the vehicle around in preparation for reentry. After the retroburn, it is necessary to turn 180 deg. for the reentry. The vehicle has to be able to do the turn before the vehicle reaches the atmosphere. The propulsion designer needs to look at the amount of RCS needed to do this turn, and do some guessing to size the RCS system. The time available for the turn should be estimated based on information from the trajectory people. The turn can readily be computed using the torque-angular-momentum equation to get the angular acceleration. A bang-bang constant-torque approximation will give a conservative estimate of the torque required. Include a safety factor in your estimates.

Although the RCS system is used for translation as well as rotation, we will not design translation motions in 450. The vehicle requires 4 thrusters in the pitch plane to achieve both signs of rotation. In addition, redundant thrusters should be provided at each position, so the vehicle does not become catastrophically unmaneuverable. In each of the 3 planes you thus need 8 thrusters, for a total of 24. It is very difficult to estimate the amount of propellant one might need, so the RFP gives the ΔV requirement from which the needed propellant can be determined.

9   Other Design Information from Gus

Following is some miscellaneous design information from my notes from the last time Prof. Gustafson taught 451.

1. Yaw Stability: could use a vertical tail, but will mostly be shadowed. Could use outboard fins, but these create a heating issue. RCS system is mostly used for yaw control on hypersonic vehicles. (1/29/98)

2. The electronics package must be in the pressurized cabin, for thermal control. (1/29/98)

3. Life Support: Need oxygen and nitrogen, with pressure regulated into the cabin. Find out on the internet how much a person consumes. If the vehicle is opened then the cabin will have to be repressurized. Use lithium canisters to remove carbon dioxide, as on the shuttle. Get a basic idea of the amount needed, and allow for the mass and volume.

4. Aerodynamics:

   (a) For a flat surface the force acts at the centroid. (2/5/98 p.5)

5. Structures/TPS:

(a) For the TPS, the specific heat c_p is temperature dependent. Fit a curve to this data and use the local value of $c_p(T)$. (2-26 p. 3)

(b) The internal temperature of the aluminum Shuttle has to be held below 350 (F?). Will see a peak temperature during reentry, perhaps at 70-80km, then temperature will drop. For some trajectories the total heat load can be an issue, but usually not (3-26).

6. Orbital Intercept: The period of an inner circular orbit is less than that of an outer orbit. To get in the right relative position to intercept, can circularize in a larger or smaller orbit and then wait a bunch of orbits. (2-26 p. 4) Four ΔV's: drop orbit, circularize, wait, raise orbit, circularize. Instead, can go to an elliptic orbit, but have to hit target. Choose period of elliptic orbit by major axis, wait to line up. Then one ΔV to start, another to circularize when arrive at target. (3/5 p. 3)

10   Some References

1. J.D. Anderson, *Hypersonic and High-Temperature Gas Dynamics*, (HHTG for short), McGraw-Hill, New York, 1989. Reprinted by AIAA Publications, Fall 2000.

2. H. Ashley, *Engineering Analysis of Flight Vehicles*, Dover, New York, 1992.

3. R.D. Bate, D.D. Mueller, and J.E. White, *Fundamentals of Astrodynamics*, Dover, New York, 1971.

4. G.F. Franklin, J.D. Powell, and A. Emani-Naeini, *Feedback Control of Dynamic Systems*, 2nd edition, Addison-Wesley, 1991.

5. Gnoffo, P.A., *Planetary-Entry Gasdynamics*, in *Annual Reviews of Fluid Mechanics*, v. 31, pp. 459-494, 1999. Surveys overall issues and computational methods.

6. M.D. Griffin and J.R. French, *Space Vehicle Design*, AIAA Education Series, 1991.

7. R.W. Humble, G. N. Henry, and W.J. Larsen, *Space Propulsion Analysis and Design*, McGraw-Hill, New York, 1995.

8. S.J. Isakowitz, J.P. Hopkins, Jr., and J.B. Hopkins, *International Reference Guide to Space Launch Systems*, Third Edition, AIAA Publications, Virginia, 1999.

9. Kinney, David J., J.V. Bowles, L.H. Yang, and C.D. Roberts, *Conceptual Design of a 'SHARP' CTV*, AIAA Paper 2001-2887, June 2001. Good introduction to preliminary or conceptual design, discussion of methods, for a high L/D vehicle with a UHTC nose.

10. Penland, J.A., J.L. Dillon, and J.L. Pittman, *An aerodynamic analysis of several hypersonic research airplane concepts from Mach 0.2 to 6.0*, AIAA Paper 78-150, Jan. 1978. General consideration of aerodynamic design issues, including static-stability margins and minimum lift coefficient for landing.

11. Rathbone, Robert R., *Communicating technical information; a new guide to current uses and abuses in scientific and engineering writing*, Addison-Wesley, 1985. On reserve in the Engineering Library.

12. Reuther, James et al., *A reusable space vehicle design study exploring sharp leading edges*, AIAA Paper 2001-2884, June 2001. One of several papers from the 35th Thermophysics meeting reporting design studies for a crew return vehicle, and exploring use of UHTC TPS and sharp leading edges.

13. Papadopoulos, P., D. Prabhu, D. Olynick, Y.K. Chen, and F.M. Cheatwood, *CFD code comparisons for Mars entry simulations*, AIAA Paper 98-0272, Jan. 1998. Recent analysis of Mars aeroheating, shows typical approach.

14. G.P. Sutton, *Rocket Propulsion Elements*, John Wiley and Sons, New York, 1992.

15. Special Section: Planetary Entry Systems (Aeroassist Systems), Journal of Spacecraft and Rockets, v. 36, n. 3, May-June 1999.

16. Special Section: HL-20 Personnel Launch System, Journal of Spacecraft and Rockets, v. 30, n. 5, Sept.-Oct. 1993. 114 pages of discussion of preliminary design of a crew return vehicle for the Space Station. Good reference for design methods, subsystem weights, etc.